JOURNAL OF GEOPHYSICAL RESEARCH, VOL. 104, NO. C1, PAGES 1465–1488, JANUARY 15, 1999

Eulerian drift induced by progressive waves above rippled and very rough beds

A. G. Davies

School of Ocean Sciences, University of Wales (Bangor), Anglesey, United Kingdom

C. Villaret[1]

Laboratoire National d'Hydraulique, E.D.F., Chatou, France

Abstract. A simple, practical, analytical model is developed of the drift induced by weakly asymmetrical progressive waves in the bottom boundary layer above rippled and very rough beds. Above such beds, momentum transfer is dominated not by random turbulence, but by the well-organized process of vortex shedding, which is characterized here by a strongly time-varying "convective" eddy viscosity K. The one-dimensional wave boundary layer model proposed is consistent with the presence of Stokes' second-order waves in the free-stream flow. The solution for the Eulerian drift is characterized by a pronounced near-bed jet in the direction of wave advance, beneath a layer extending to the edge of the boundary layer in which the drift is in the opposite direction. An empirical approach involving five published laboratory data sets is used to estimate the coefficient defining the asymmetrical time-varying component of K above rippled and very rough beds. The resulting "standard" model is then compared both with measurements of the drift at the edge of the wave boundary layer and also with measured drift profiles. Good agreement is found for ranges of wave steepness and relative bed roughness of practical importance.

1. Introduction

The accuracy of models of coastal sediment transport depends upon reliable parameterizations of detailed hydrodynamic processes. However, these processes are not always well understood. For example, the presence of small, near-bed, wave-induced currents has been shown to have a large effect upon the net sediment transport rate beneath asymmetrical waves [*Davies and Li*, 1997]. Such currents necessarily affect also the vertical profile of the residual current in the water column as a whole, since the near-bed streaming provides the bottom boundary condition for this profile (e.g., *Longuet-Higgins*' [1953] "conduction solution"). However, the magnitude and even direction of such near-bed currents are sometimes uncertain, and their effects are often not included in models. This raises questions of fundamental interest, as well as practical importance for applied work.

Most previous studies of near-bed drift have been concerned with smooth beds or flat rough beds, for which concepts derived from steady turbulent boundary layer flow remain applicable (see the review of *Davies and Villaret* [1997]). The effect of vertical velocities induced in the bottom boundary layer by progressive waves was first explained theoretically by *Longuet-Higgins* [1953], who showed that, at the edge of the laminar boundary layer above a smooth flat bed, the Eulerian drift $\overline{U}_{\infty y}$ is given to a first approximation by $\overline{U}_{\infty y} c/U_0^2 = 0.75$, where c is the wave phase speed and U_0 is the near-bed velocity amplitude. This classical result has been shown to agree with measurements made above smooth beds in laminar conditions, at least for low waves [e.g., *Brebner et al.*, 1966]. *Longuet-Higgins* [1958] also argued that, subject to the assumption of a time- and height-invariant eddy viscosity K, the normalized drift at the edge of the turbulent boundary layer above a smooth bed should still equal 0.75, and, in fact, this result remains valid even if height variation is introduced into K [e.g., *Johns*, 1970].

However, experimental and theoretical studies involving flat rough beds in the turbulent flow regime have shown that the near-bed drift depends rather critically upon the bed roughness, as well as on the degree of wave asymmetry. The effect of bed roughness is to reduce the phase lead of the bottom velocity in comparison with the lead of $\pi/4$ given by the classical Stokes' solution. This causes the Eulerian drift to be reduced (i.e., $\overline{U}_{\infty y} c/U_0^2 < 0.75$), as shown by *Trowbridge and Madsen* [1984b], whose two-layer eddy viscosity model included both height variation in K and also a reference elevation (i.e., bed roughness length scale $z_0 = k_s/30 > 0$). (It should be noted that a very different behavior is found in the transitional flow regime, where a strong enhancement in the nondimensional drift may be expected, at least for low values of the wave Reynolds number [*Davies and Villaret*, 1998].)

In addition to the drift associated with the vertical velocity field, any asymmetry in the turbulence intensity in successive wave half cycles will give rise to a near-bed residual current component. For a plane bed, this component is in the offshore direction as demonstrated, in isolation from other processes,

[1] Also at School of Ocean Sciences, University of Wales (Bangor), Anglesey, United Kingdom.

Paper number 1998JC900016.
0148-0227/99/1998JC900016$09.00

by *Ribberink and Al Salem* [1995] for asymmetrical waves in an oscillating water tunnel [see *Davies and Li*, 1997]. These two competing mechanisms were considered by *Trowbridge and Madsen* [1984b], whose model included an asymmetrically time-varying eddy viscosity. In this and other modeling studies, it has been found that, above flat rough beds, the effect of asymmetry in the turbulence in successive half cycles is to reduce the Eulerian drift, with a reversal in the direction of drift occurring for very long waves.

The present study is concerned with the prediction of residual currents generated in the turbulent wave boundary layer above very rough and rippled beds. In this regime ($A_0/k_s \lesssim 5$, where A_0 is near-bed excursion amplitude and k_s is equivalent bed roughness), momentum transfer in the near-bed layer is dominated not by random turbulent processes, but by more organized, spatially and temporally coherent structures, resulting from the shedding of vortices from bed roughness elements at flow reversal. This complex two- (or three-) dimensional process can be represented by discrete vortex models [e.g., *Block et al.*, 1994; *Perrier*, 1996]. However, in order to simplify the problem for practical purposes, *Davies and Villaret* [1997] (hereafter referred to as DV97) adopted a simpler one-dimensional, horizontally averaged description of the flow. This analysis, based on spatial-mean quantities, was suggested by the experimental work of *Ranasoma* [1992] [see also *Ranasoma and Sleath*, 1992]. Here local, phase-averaged measurements of horizontal velocity and momentum transfer were made above rippled beds in symmetrical oscillatory flow, and the results were then horizontally averaged at various elevations above the ripple crest level. From an analysis of the resulting mean velocity field, Ranasoma and Sleath concluded that, close to the bed, large-scale mixing produced by vortices had the dominant effect on the mean velocity profiles, whereas at distances from the bed greater than about two ripple heights, turbulence had the dominant effect. Noting that the measured spatial-mean velocity profiles preserved features of the classical Stokes' shear wave solution, DV97 suggested that the problem might be analyzed quite simply using standard gradient diffusion arguments. In particular, they defined a time-varying "convective" eddy viscosity to relate the horizontally averaged total shear stress, due mainly to periodic velocity contributions, to the horizontally averaged mean flow velocity gradient. This approach clearly does not provide any insight into the details of the flow in between roughness elements. However, its validity was confirmed by *Perrier* [1996], who horizontally averaged the results of a two-dimensional (2-D) discrete vortex model of oscillatory flow over a rippled bed [*Perrier et al.*, 1994] and hence recovered the essential structure of the present one-dimensional (1-D) time-varying eddy viscosity from the computed shear stress and mean velocity fields.

A parameterization of both the mean and time-varying components of the convective eddy viscosity was obtained by DV97 from a detailed analysis of *Ranasoma*'s [1992] data. They found that the maximum value of K during each wave half cycle occurred at the phase angle of flow reversal, and that the relative amplitude of the (symmetrical) time-varying component of K was of the same order of magnitude as the mean component. In a previous study, *Sleath* [1991] adopted an analogy with grid turbulence and suggested use of a time- and height-invariant eddy viscosity in very rough turbulent flow conditions. In fact, the formula proposed by Sleath was found by DV97 to be in reasonable agreement with the mean (time averaged) component of K, which they had estimated from Ranasoma's laboratory data. A similar time- and height-invariant eddy viscosity formula was suggested by *Nielsen* [1992], though for somewhat rougher flow conditions. Following *Sleath* [1991] and *Nielsen* [1992], DV97 assumed, as a first approximation, that both the mean and time-varying components of the convective eddy viscosity should remain constant with height above the bed. They noted also that the peak values of K given by this model during the wave cycle were comparable in magnitude with the constant values of K determined independently by *Ranasoma and Sleath* [1992] for the outer turbulent flow in their experiments.

For symmetrical waves, the effect of the above time-varying eddy viscosity is to alter the phase relationship between the horizontal and vertical components of velocity within the bottom wave boundary layer. This causes a reduction in the near-bed drift of the kind observed qualitatively by *Bijker et al.* [1974], who found that when the same incident waves propagated above a smooth bed, then above a flat, sand-roughened, bed and, finally, above a rippled bed, the onshore near-bed drift was reduced in magnitude above the sand bed, and then further reduced to approximately zero above the rippled bed. This behavior has been confirmed in several more recent quantitative studies.

The predictions of the DV97 model were tested by *Davies and Villaret* [1998] (hereafter referred to as DV98) against four published data sets obtained in the rough turbulent regime. Their main conclusion was that the predictions of the model systematically underestimated the reduction in the near-bed drift (i.e., compared with *Longuet-Higgins*' [1953] result). This was attributed to the fact that all the data considered had been obtained beneath waves displaying some degree of asymmetry, which caused shedding of vortices of unequal strength in successive wave half cycles above the rippled and very rough beds in question. In fact, it was shown qualitatively by DV98 that the effects of wave asymmetry, which were not included in the DV97 model, played a major, complementary role in determining the near-bed drift.

Our aim in this paper is to extend the DV97 convective eddy viscosity model by including the effects of wave asymmetry, and to examine the implications of this model for the drift within the wave boundary layer. In section 2 we introduce the time-varying eddy viscosity K used to represent momentum transfer due to vortex shedding. Here also we discuss the "spatially-averaged" boundary layer equation and obtain equations at first and second order in a scheme consistent with classical Stokes' theory. In section 3, these equations are solved using a standard perturbation approach in which both symmetrical and asymmetrical time-varying components of K are assumed to be small. In section 4 we then obtain the solution for the Eulerian drift, and discuss the behavior of its different components as the degree of wave asymmetry B (equation (29)) and the nonlinearity parameter c/U_0 are varied. In section 5, an empirical approach, based on five published experimental data sets, is used to estimate the coefficient defining the asymmetrical time-varying component of K. The model predictions are then compared both with measurements of the drift at the outer edge of the wave boundary layer and also with measured drift profiles. In section 6 the results are discussed, and the dependence of the model coefficients on the degree of wave asymmetry as well as on the relative roughness of the bed are considered. In section 7 the conclusions are stated.

2. Formulation

2.1. Governing Equations

We consider the flow induced in the bottom boundary layer by progressive, monochromatic waves traveling in water of constant mean depth. At the edge of the oscillatory boundary layer, the unsteady component of the motion is assumed to be described by the classical Stokes' second-order solution for inviscid, irrotational flow. The bed is assumed to be fixed and very rough, the roughness elements being either three-dimensional grains or two-dimensional ripples. In each case the boundary layer flow is assumed to be nonlaminar, being influenced in the former case and dominated in the latter case by spatially and temporally well-organized vortex shedding events.

In models of rough turbulent boundary layer flow it is normally assumed that the boundary layer thickness is large compared with the scale of the bed roughness, such that there exists a region inside the boundary layer that is not influenced directly by the flow past individual roughness elements. In order to retain the simplicity of a one-dimensional model based on the gradient diffusion concept, this assumption is made here, even for the case of rippled beds above which vortex shedding gives rise to complicated two-dimensional flow structures extending through much of the boundary layer. In the model described below, we aim to capture the essential physics of the 2-D vortex shedding phenomenon within a simple, locally 1-D model.

Initially, we extend the formulation discussed by DV97 by the inclusion of nonlinear convective terms in the free-stream flow at the edge of the boundary layer. In DV97 the instantaneous, local, horizontal, and vertical components of velocity u,w in the two-dimensional boundary layer flow were decomposed into phase-averaged u_p,w_p and turbulent u',w' components, such that $u = u_p + u'$ and $w = w_p + w'$. If viscous stresses are neglected and convective terms are included in the free stream, the phase-averaged momentum balance in the horizontal x -direction (the direction of wave travel) may be expressed [cf. *Nielsen*, 1992] as

$$\frac{\partial u_p}{\partial t} + u_p\frac{\partial u_p}{\partial x} + w_p\frac{\partial u_p}{\partial z} = \frac{\partial u_\infty}{\partial t} + u_\infty\frac{\partial u_\infty}{\partial x} - \frac{\partial}{\partial x}(u'^2)_p - \frac{\partial}{\partial z}(u'w')_p \ . \qquad (1)$$

Here z is positive in the upward direction with $z = 0$ at the bed; time is denoted by t, u_∞ is the free-stream velocity; and $(u'^2)_p$ and $(u'w')_p$ are the normal and tangential components, respectively, of the phase-averaged turbulent Reynolds stress. The velocity components u_p,w_p are related by the continuity equation

$$\frac{\partial u_p}{\partial x} + \frac{\partial w_p}{\partial z} = 0 \ . \qquad (2)$$

For a rippled bed of wavelength λ which is much smaller than the surface wavelength λ_s, the velocity components u_p,w_p may be horizontally averaged locally (i.e., over one ripple wavelength) such that

$$u_p = \langle u_p\rangle + \tilde{u}_p \ , \quad w_p = \langle w_p\rangle + \tilde{w}_p \ , \qquad (3)$$

where

$$\langle u_p\rangle = \frac{1}{\lambda}\int_{x-\lambda/2}^{x+\lambda/2} u_p\,dx \ , \quad \langle w_p\rangle = \frac{1}{\lambda}\int_{x-\lambda/2}^{x+\lambda/2} w_p\,dx \ , \qquad (4)$$

and $\tilde{u}_p,\tilde{w}_p$ represent the variations in velocity occurring within one wavelength (with $\langle\tilde{u}_p\rangle = \langle\tilde{w}_p\rangle = 0$). This averaging procedure may be extended to three-dimensionally rough beds by the choice of a suitably large averaging length. After local averaging, the horizontal variations in $\langle u_p\rangle$ and $\langle w_p\rangle$ that remain are due solely to the changes that occur on the larger scale of the surface wavelength.

After (3) is substituted into (1) and (2) and local averaging has been carried out, the momentum equation (1), subject to the boundary layer approximation, may be written as

$$\frac{\partial\langle u_p\rangle}{\partial t} + \langle u_p\rangle\frac{\partial\langle u_p\rangle}{\partial x} + \langle w_p\rangle\frac{\partial\langle u_p\rangle}{\partial z} = \frac{\partial u_\infty}{\partial t} + u_\infty\frac{\partial u_\infty}{\partial x} + \frac{1}{\rho}\frac{\partial\tau_p}{\partial z} \ , \qquad (5)$$

where ρ is the fluid density, and the shear stress τ_p is given by

$$\tau_p = -\rho\langle(u'w')_p\rangle - \rho\langle\tilde{u}_p\tilde{w}_p\rangle \ . \qquad (6)$$

The total stress τ_p in (6) is made up of two components. The first is the horizontally averaged turbulent Reynolds stress, and the second is the horizontally averaged momentum transfer by periodic velocity correlations, which makes the dominant contribution to τ_p above rippled (and very rough) beds [cf. *Sleath,* 1987]. The eddy viscosity K which relates the total shear stress to the horizontally averaged velocity gradient is defined by

$$\tau_p = \rho K\frac{\partial\langle u_p\rangle}{\partial z} \ . \qquad (7)$$

As has often been pointed out [e.g., *Rodi*, 1984], the eddy viscosity analogy between turbulent and molecular motion cannot be correct, in principle, because the "free paths" of the larger eddies responsible for momentum transfer are not small compared with the fluid domain. Indeed, this objection to the use of gradient diffusion concepts might be considered particularly relevant here. However, our aim is to demonstrate that the eddy viscosity K as defined by (7) provides a good practical tool with which to analyze the spatial-mean flow.

The unsteady component of u_∞ is assumed to be described by Stokes' second-order solution evaluated at $z = 0$, while the steady component is determined by the mechanics of the boundary layer and so is unknown at the outset. At the edge of the boundary layer, $\langle u_p\rangle$ tends to u_∞, while τ_p decreases to zero. At the theoretical bed level, located between the crests and troughs of the bed roughness elements, the flow is assumed to satisfy the no-slip condition ($\langle u_p\rangle = \langle w_p\rangle = 0$ at $z = 0$). Finally, the locally averaged continuity equation that must be satisfied by the two-dimensional boundary layer flow is

$$\frac{\partial\langle u_p\rangle}{\partial x} + \frac{\partial\langle w_p\rangle}{\partial z} = 0 \ . \qquad (8)$$

In the boundary layer approximation (5) to the momentum equation, the terms neglected are $O(k\delta)$ compared with the leading terms, which comprise the linear terms (including the stress term), while the nonlinear convective terms in (5) are $O(kA_0)$ compared with these leading terms. (Here k is the

surface wavenumber and δ is the boundary layer thickness.) Since in Stokes' solution the quantity (kA_0) is assumed to be small compared with unity, this allows a series solution to be written, as follows:

$$\begin{aligned} u_\infty &= u_{\infty 1} + u_{\infty 2} + \ldots. \\ \langle u_p \rangle &= u_1 + u_2 + \ldots. \\ \langle w_p \rangle &= w_1 + w_2 + \ldots. \\ \tau_p &= \tau_1 + \tau_2 + \ldots. \end{aligned} \quad , \tag{9}$$

where quotients such as u_2/u_1 are $O(kA_0)$. Substitution of (9) into (5) and (8) yields the following linear equations at leading order $[O(kA_0)]$:

$$\frac{\partial u_1}{\partial t} = \frac{\partial u_{\infty 1}}{\partial t} + \frac{\partial}{\partial z}\left(\frac{\tau_1}{\rho}\right) \tag{10a}$$

$$\frac{\partial u_1}{\partial x} + \frac{\partial w_1}{\partial z} = 0 \; . \tag{10b}$$

At second order $[O(kA_0)^2]$, the following equations are obtained

$$\frac{\partial u_2}{\partial t} + u_1\frac{\partial u_1}{\partial x} + w_1\frac{\partial u_1}{\partial z} = \frac{\partial u_{\infty 2}}{\partial t} + u_{\infty 1}\frac{\partial u_{\infty 1}}{\partial x} + \frac{\partial}{\partial z}\left(\frac{\tau_2}{\rho}\right) \tag{11a}$$

$$\frac{\partial u_2}{\partial x} + \frac{\partial w_2}{\partial z} = 0 \; . \tag{11b}$$

The unsteady components of horizontal velocity at the outer edge of the wave boundary layer, consistent with (10) and (11), are given by

$$u_{\infty 1} = U_0 \cos\theta \tag{12a}$$

$$u_{\infty 2} - \overline{u_{\infty 2}} = \frac{3kA_0}{4\sinh^2 kh} U_0 \cos 2\theta \; , \tag{12b}$$

where $U_0 = A_0\omega$ is the free-stream velocity amplitude, $\theta = (\omega t - kx)$ is the wave phase function in which ω is the angular frequency and h is the water depth. The overbar denotes time-averaging over one wave period.

Finally, in anticipation of the constrained relationship between the even and odd harmonics in the solution, it is convenient to write:

$$K = K_{even} + K_{odd} \; , \tag{13}$$

where K_{even} and K_{odd} include, respectively, the even and odd harmonic contributions to the time-varying eddy viscosity K. The resulting first- and second-order stress fields are then given by

$$\tau_1 = \rho K_{even}\frac{\partial u_1}{\partial z} \tag{14a}$$

$$\tau_2 = \rho K_{even}\frac{\partial u_2}{\partial z} + \rho K_{odd}\frac{\partial u_1}{\partial z} \; . \tag{14b}$$

Hereafter, we use complex notation, replacing the various (lower case) variables in (9) by the real parts of (upper case) variables defined by $u_1 = \mathrm{Re}\,(U_1 e^{i\theta})$, etc.

2.2. Time-Varying Eddy Viscosity

For the specification of the eddy viscosity within the oscillatory boundary layer above rippled (or very rough) beds, we follow DV97 and define a "convective eddy viscosity" which exhibits time t dependence but no height z dependence as follows:

$$K = \tfrac{1}{2}K_0\left[1 + \varepsilon_1 e^{i\theta} + \varepsilon_2 e^{2i\theta}\right] , \tag{15a}$$

so that

$$K_{even} = \tfrac{1}{2}K_0\left[1 + \varepsilon_2 e^{2i\theta}\right] , \qquad K_{odd} = \tfrac{1}{2}K_0\varepsilon_1 e^{i\theta} . \tag{15b}$$

As noted in section 1, the leading constant term ($\frac{1}{2}K_0$) on the right hand side of (15a) may be calculated using the formula of either *Sleath* [1991] or *Nielsen* [1992] (see section 5.2.2). The second term represents the time variation in K which occurs at the first harmonic frequency as a result of asymmetry in the free-stream flow (equation (12)). The magnitude of the complex coefficient $\varepsilon_1 = |\varepsilon_1|\exp(i\varphi_1)$ might therefore be expected to be small, though we leave open the possibility that it is $O(1)$; its phase angle φ_1, which is governed by the eddy-shedding process at the bed level, is discussed in section 5.2.1. The third term on the right-hand side of (15a) represents symmetrical time variation in the convective eddy viscosity, which also occurs as a result of eddy shedding from the bed in each wave half cycle. The magnitude of the coefficient $\varepsilon_2 = |\varepsilon_2|\exp(i\varphi_2)$ is not prescribed at the outset; in fact, from an analysis of the rippled bed data of *Ranasoma* [1992], it has been shown by DV97 to be $O(1)$. Initially therefore we leave open the possibility that $|\varepsilon_2|$ is either small or $O(1)$. As far as the phase angle φ_2 is concerned, this has been shown by DV97 to be governed by the phase of eddy shedding at flow reversal (see section 5.2.1).

The truncation of the expression for K at the third harmonic frequency is not intended to imply that time variation in the eddy viscosity is nonexistent at frequencies higher than the second. However, it has been shown by DV97 that the contribution to the solution for the velocity field arising from the fourth and higher (even) harmonics in K is relatively small. Thus, in order to preserve simplicity while still capturing the essential consequences of the eddy-shedding process, we have adopted the simple form for K given by (15).

3. Perturbation Solution Scheme

3.1. Structure of Solution

The structure of the perturbation solution is shown in Table 1. Essentially, we treat (kA_0) as the small parameter which establishes the basic hierarchy in the solution (see (9)). The solutions obtained at both first $[O(kA_0)]$ and second $[O(kA_0)^2]$ order are then perturbed by the terms in (15) involving ε_1 and ε_2, which define the time variation in K. In other words, we treat ε_1 and ε_2 as secondary perturbation parameters and, initially at least, neglect terms involving squares and products of these quantities at each order of the basic solution defined by (kA_0).

As noted in section 2.2, there is some uncertainty about the magnitude of ε_2 (and also ε_1). The possibility that $|\varepsilon_2|$ is $O(1)$ has been discussed by DV97, who compared the present perturbation solution with a coupled solution based on the method of normal modes (see the appendix). This comparison, which showed close agreement between the amplitude and phase of the fundamental component of velocity, even if $|\varepsilon_2|$ is $O(1)$, provides independent support for the development here of a relatively simple practical model involving the secondary perturbation parameters. For completeness, however, we note later both the effect of retaining $\sim|\varepsilon_2|^2$ terms in the lowest-order velocity solution and the effects of retaining terms involving squares and products of ε_1 and ε_2 in the

Table 1. Summary of the Perturbation Solution Scheme for the Velocity Field and the Eulerian Drift

Order of Basic Solution for Velocity Field	Perturbations to Velocity Field	Order of Contributions to Eulerian drift
First harmonic $O(kA_0)$	$O(\varepsilon_2)$, equation (21)[a] basic Stokes' solution, (18)	wave Reynolds stress terms on right hand side of (32): $O(kA_0)^2$ and perturbation $O[(kA_0)^2\,\varepsilon_2]$, (39) and (42)[b] asymmetry terms: $O\,[\varepsilon_1(kA_0)]$, (46)[c]
Second harmonic $O(kA_0)^2$	none[d] basic Stokes' solution, (30)	wave Reynolds stress terms: none since $O(kA_0)^4$ terms negligible asymmetry term: $O[\,\varepsilon_2(kA_0)^2]$, (48)

Here k is the surface wavenumber and A_0 is the near-bed excursion amplitude.
[a] The complete solution correct to $O(\varepsilon_2)^2$ is given in the appendix. There is no possible ε_1 perturbation.
[b] See the appendix for additional ε_2^2 perturbation term (see (43)).
[c] See (47) for $O[\varepsilon_1\varepsilon_2(kA_0)]$ term.
[d] Any ε_2 perturbation will not contribute to the drift at order lower than $(kA_0)^4$.

final solution for the Eulerian drift. In practice, the inclusion of such terms makes a very minor adjustment to the results.

In sections 3.2 and 3.3, we obtain solutions for the velocity field at the first and second harmonic frequencies for use in the determination of the near-bed drift. In principle, since the eddy viscosity is time varying, the velocity field should contain an infinite number of harmonics. However, in practice, we concentrate on the leading terms, giving emphasis to those aspects of the solution relevant to the generation of near-bed currents. So, for example, the contribution of the velocity field at the third harmonic frequency has been neglected, even though the behavior of the third (and also fifth) harmonic was used by DV97 to determine the form of the time-varying eddy viscosity K in (15).

3.2. First-Order Solution

We seek initially the lowest-order $[O(kA_0)]$ solution of (10a) at the first harmonic (fundamental) frequency, and then obtain the perturbation to this solution resulting from the (small) term of order $|\varepsilon_2|$ in the convective eddy viscosity (15) (see Table 1). As a result of the distinct roles of the odd and even harmonics in K, it is only the term $\sim\varepsilon_2$ which contributes a perturbation to the lowest-order component of the velocity u_1.

If we write

$$u_1 = U_1 e^{i\theta}, \quad u_{\infty 1} = U_0 e^{i\theta} \tag{16}$$

and then substitute (14a) into (10a), subject to (15), the momentum equation $O(kA_0)$ at the first harmonic frequency ($\sim e^{i\theta}$) becomes

$$\frac{i\omega}{2}U_1 = \frac{i\omega}{2}U_0 + \frac{K_0}{4}\left[\frac{\varepsilon_2}{2}\frac{d^2U_{1*}}{dz^2} + \frac{d^2U_1}{dz^2}\right], \tag{17}$$

in which the asterisk denotes the complex conjugate. In the absence of ε_2 time variation in (17), the solution for $U_1(z)$ ($=U_{11}$, say) that satisfies the no-slip condition at $z = 0$ reduces to the familiar Stokes' shear wave solution, namely,

$$U_{11} = U_0\left[1 - e^{-(1+i)\alpha z}\right], \tag{18}$$

where $\alpha = (\omega/K_0)^{1/2}$ is the wavenumber that characterizes the decay rate of the shear wave with height above the bed. If the ε_2 term is reintroduced and a solution of (17) is sought which represents a perturbation of (18) such that

$$U_1 = U_{11} + U_{12}, \tag{19}$$

where $U_{12}(z)$ is $O(\varepsilon_2)$, then U_{12} must satisfy

$$\frac{d^2U_{12}}{dz^2} - \frac{2i\omega}{K_0}U_{12} = -\frac{\varepsilon_2}{2}\frac{d^2U_{11*}}{dz^2}, \tag{20}$$

in which U_{11} is given by (18). In order to satisfy the no-slip condition, the particular solution of (20) must be combined with the solution of the homogeneous equation for U_{12}, yielding the following solution for U_1:

$$U_1 = U_0\left[1 - e^{-(1+i)\alpha z} + \frac{\varepsilon_2}{4}e^{-(1-i)\alpha z} - \frac{\varepsilon_2}{4}e^{-(1+i)\alpha z}\right]. \tag{21}$$

The corresponding solution ($O(\varepsilon_2)$) for the velocity component U_3 at the third harmonic frequency has been discussed by DV97. They found that $|U_3/U_1|$ remains small, even if $|\varepsilon_2|$ is $O(1)$, as a result of the constraint of the upper and lower boundary conditions.

3.3. Second-Order Solution

The second-order solution for the velocity field satisfying (11) and (12) is obtained by arguments similar to those used by *Trowbridge and Madsen* [1984b]. With an eye on the objective of this paper, namely, the determination of the near-bed residual current field, we anticipate that a second-order solution that is consistent with the present small parameter approach requires K_{even} in (15b) to be taken equal to only the time-invariant component of the eddy viscosity, namely, $\frac{1}{2}K_0$. In other words, the second harmonic contribution to K in (15a) may be neglected. As far as the first harmonic contribution is concerned, this may be retained through the second-order stress field (equation (14b)). However, the contribution ultimately made by this term to the residual current field is strictly of higher order. If the second harmonic in K is neglected in calculating u_2, the lowest order velocity field for use in (11a) becomes simply the Stokes' shear wave solution U_{11}

given by (18), and the corresponding lowest-order shear stress τ_{11}, say, is given by (14a) in which $K_{even} = \frac{1}{2}K_0$.

At the outset we need to eliminate w_1 from (11a) by using (10). For progressive waves, integration of (10b) yields

$$w_1 = -\int_0^z \frac{\partial u_1}{\partial x} dz = +\frac{k}{\omega}\int_0^z \frac{\partial u_1}{\partial t} dz , \qquad (22)$$

and so, after using (10a),

$$w_1 = \frac{k}{\omega}\frac{\partial u_{\infty 1}}{\partial t} z + \frac{k}{\omega}\left[\frac{\tau_1}{\rho} - \frac{\tau_{b1}}{\rho}\right], \qquad (23)$$

in which τ_{b1} represents the lowest-order bed shear stress and in which we take $\tau_1 = \tau_{11}$ for the reason given above. After substituting (23) into (11a), the second-order momentum equation may be written in the form:

$$-\frac{\partial u_2}{\partial t} + \frac{\partial}{\partial z}\left[\frac{\tau_2}{\rho}\right] = -\frac{\partial u_{\infty 2}}{\partial t} + \frac{1}{2}\frac{\partial}{\partial x}(u_{\infty 1} - u_1)^2 - \frac{\partial}{\partial x}\left[u_{\infty 1}(u_{\infty 1} - u_1)\right] + \frac{k}{\omega} z \frac{\partial u_{\infty 1}}{\partial t}\frac{\partial u_1}{\partial z} + \frac{k}{\omega}\frac{\partial u_1}{\partial z}\left[\frac{\tau_1}{\rho} - \frac{\tau_{b1}}{\rho}\right]. \qquad (24)$$

The second-order velocity and stress fields each comprises a second harmonic component and a time-mean component (denoted by an overbar) as follows:

$$u_2 = \left[\overline{u_2} + U_2 e^{2i\theta}\right], \qquad \tau_2 = \left[\overline{\tau_2} + T_2 e^{2i\theta}\right]. \qquad (25)$$

For consistency with the notation adopted in obtaining the first-order solution, we denote by u_{21} and τ_{21}, respectively, the second-order velocity and stress components derived subject to the assumption of a time-invariant eddy viscosity (i.e., $K_{even} = \frac{1}{2}K_0$), such that

$$\overline{\tau_{21}} = \tfrac{1}{2}K_0\rho\frac{d\overline{u_{21}}}{dz}, \qquad T_{21} = \tfrac{1}{2}K_0\rho\frac{dU_{21}}{dz}. \qquad (26)$$

If the ε_1 term is retained at this stage, this has no effect at lowest order on solution (30). We therefore delay the introduction of this term until section 4, where the drift velocity is calculated.

After substituting (25) into (24) and collecting the terms at the second harmonic frequency, the equation governing U_{21} becomes

$$\frac{d}{dz}\left[\tfrac{1}{2}K_0\frac{dU_{21}}{dz}\right] - 2i\omega U_{21} = -2i\omega U_{\infty 2} + ikU_{\infty 1}\left[U_{\infty 1} - U_{11}\right] - \frac{ik}{2}\left[U_{\infty 1} - U_{11}\right]^2 + \tfrac{1}{2}ikU_{\infty 1} z\frac{dU_{11}}{dz} + \tfrac{1}{2}\frac{k}{\omega}\frac{dU_{11}}{dz}\left[\frac{T_{11}}{\rho} - \frac{T_{b11}}{\rho}\right]. \qquad (27)$$

The terms on the right-hand side of (27) are known from (18) and (14a), in which $U_1 = U_{11}$ and $K_{even} = \frac{1}{2}K_0$ in the calculation of $\tau_{11} = T_{11}e^{i\omega t}$. If, for convenience, (12b) is rewritten

$$u_{\infty 2} - \overline{u_{\infty 2}} = BU_0 e^{2i\theta}, \qquad (28)$$

so that

$$U_{\infty 2} = BU_0 \qquad (29)$$

where $B = \frac{3}{4}kA_0/\sinh^2 kh$, then, after some algebra, the solution for U_{21}, which satisfies the no-slip condition on $z = 0$, becomes

$$U_{21} = U_0\left\{B - \tfrac{1}{2}\frac{k}{\omega}U_0\left[1 + \alpha z(1+i)\right]e^{-\alpha(1+i)z} + \left(-B + \tfrac{1}{2}\frac{k}{\omega}U_0\right)e^{-\sqrt{2}(1+i)\alpha z}\right\}. \qquad (30)$$

4. Eulerian Drift in the Bottom Boundary Layer

4.1. Mean Momentum Balance and Drift Profile

The near-bed drift $\bar{u}_2$ results from contributions (see Table 1) arising from the relationship between the time-varying velocity field, which has been determined earlier to first and second order with respect to (kA_0) (equations (21) and (30), respectively) and the time-varying eddy viscosity K given by (15). If, following substitution of (25) into (24), the time-mean momentum balance is obtained and this equation is integrated with respect to z, it follows that [cf. *Trowbridge and Madsen*, 1984b]

$$\frac{\overline{\tau_2}}{\rho} = \frac{k}{\omega}z\,\overline{u_1\frac{\partial u_{\infty 1}}{\partial t}} + \frac{k}{\omega}\overline{u_1\left(\frac{\tau_1}{\rho} - \frac{\tau_{b1}}{\rho}\right)} + \frac{k}{\omega}\overline{u_{\infty 1}\frac{\tau_{b1}}{\rho}}. \qquad (31)$$

By use of (23), this may be expressed alternatively as

$$\frac{\overline{\tau_2}}{\rho} = \overline{u_1 w_1} - \overline{(u_1 w_1)_\infty}. \qquad (32)$$

It is (32) which most clearly expresses the essential physics of the time-mean momentum balance in the bottom boundary layer. Note that the second-order velocity field does not contribute to the right-hand side of (32), the term $(\overline{u_2 w_2})$ being $O(kA_0)^4$.

The second-order velocity U_{21} was derived earlier, subject to the neglect of the ε_2 term in (15). In order to calculate the complete second-order stress field on the left-hand side of (32), we now reintroduce both this symmetrical ($\sim\varepsilon_2$) time variation in K, and also the asymmetrical ($\sim\varepsilon_1$) time variation. The complete second-order mean stress field then comprises the contribution $\bar{\tau}_{21}$ given by (26) together with contributions at second-order arising from the following: (1) One contribution is the leading-order component of velocity (u_{11}) at the first harmonic frequency, in combination with the ε_1 asymmetry term in K (equation (15)). Since u_{11} is $O(kA_0)$ and the eddy viscosity term is $O(\varepsilon_1)$, the resulting contribution to the mean stress is $O[\varepsilon_1(kA_0)]$. Although the ε_2 terms in the complete first-order solution (21) may not be strictly "small", we assume here initially that terms involving the product $\varepsilon_1\varepsilon_2$ are small and may be ignored. (2) A second contribution is the leading-order velocity component u_{21} at the second harmonic frequency, in combination with the ε_2 term in K. Since u_{21} is $O(kA_0)^2$ and the eddy viscosity term is $O(\varepsilon_2)$, the contribution to the mean stress is $O[\varepsilon_2(kA_0)^2]$. The justification for the neglect of ε_2 terms in the earlier derivation of u_{21} was that the resulting contribution to the mean stress field would be $O[\varepsilon_2^2(kA_0)^2]$, which is assumed to be negligible.

So the second-order mean stress arises from (the real part of) (15a) and the expression

$$U = \overline{U} + U_1 e^{i\theta} + U_2 e^{2i\theta} \qquad (33)$$

in which $\overline{U}$ (= $\bar{u}_2$) is the second-order residual velocity, U_1 is the first-order velocity amplitude which contains terms both $O(kA_0)$ and $O[\varepsilon_2(kA_0)]$ (see (21)), and $U_2 = U_{21}$ is the second-order velocity amplitude which is $O(kA_0)^2$. Assuming that terms involving squares and products of ε_1 and ε_2 are negligi-

ble, the second-order mean stress $\overline{T}_2$ ($= \bar{\tau}_2$) is given by the real part of

$$\frac{\overline{T_2}}{\rho} = \tfrac{1}{2}K_0\left[\frac{d\overline{U}}{dz} + \tfrac{1}{2}\varepsilon_1\frac{dU_{11*}}{dz} + \tfrac{1}{2}\varepsilon_2\frac{dU_{21*}}{dz}\right]. \quad (34)$$

Before substituting this expression into (32), we use (22) to express the first-order vertical velocity as

$$W_1 = \frac{i\omega}{c}\int_0^z U_1 dz, \quad (35)$$

where the phase speed $c = \omega/k$. It follows that

$$\overline{u_1 w_1} - \overline{(u_1 w_1)_\infty} = \tfrac{1}{2}U_1 W_{1*} - \tfrac{1}{2}(U_1 W_{1*})_\infty = \frac{i\omega U_{1*}}{2c}\int_0^z U_1 dz - \frac{i\omega U_{\infty 1*}}{2c}\int_0^\infty U_1 dz. \quad (36)$$

After substitution of (34) and (36) into (32), the mean momentum balance may be expressed as follows:

$$\frac{K_0}{2}\frac{d\overline{U}}{dz} = \frac{i\omega}{2c}\left[U_{1*}\int_0^z U_1 dz - U_{\infty 1*}\int_0^\infty U_1 dz\right] - \frac{K_0}{2}\frac{\varepsilon_1}{2}\frac{dU_{11*}}{dz} - \frac{K_0}{2}\frac{\varepsilon_2}{2}\frac{dU_{21*}}{dz}, \quad (37)$$

in which the respective terms on the right-hand side are subject, at most, to a correction of order ε_1 or ε_2 (see Table 1). The first term arises from (32) and depends upon the vertical velocity field. The second and third terms are "asymmetry terms" arising from the first and second harmonics of the time-varying eddy viscosity, respectively, and are independent of the vertical velocity field. We now evaluate these terms in turn.

4.1.1. Term 1. This arises from the wave Reynolds stress associated with the lowest-order velocity field. Prior to the introduction of the ε_2 correction, the horizontal velocity is given by U_{11} (equation (18)). If, initially, U_{11} is substituted for U_1 in the first term on the right-hand side of (37), the basic Stokes' contribution to the Eulerian drift $\overline{U}_s$, say, is given by the real part of

$$\frac{K_0}{2}\frac{d\overline{U_s}}{dz} = \frac{i\omega}{2c}U_0^2\left[\frac{(1-i)}{\alpha}e^{-\alpha z}\cos\alpha z - ze^{-\alpha z}e^{i\alpha z} - \frac{(1-i)}{2\alpha}e^{-2\alpha z}\right], \quad (38)$$

which yields the following drift profile satisfying the requirement of no slip at $z = 0$ [cf. *Longuet-Higgins*, 1958]:

$$\overline{U_s} = \frac{U_0^2}{4c}\left[3 - 4e^{-\alpha z}\cos\alpha z + e^{-2\alpha z}\right] - \frac{U_0^2}{2c}\left\{\alpha z e^{-\alpha z}[\sin\alpha z + \cos\alpha z] - e^{-\alpha z}\sin\alpha z\right\}. \quad (39)$$

The lowest-order velocity field U_1 subject to the correction $O(\varepsilon_2)$ is given by (21), which may be written as

$$U_1 = U_{11} + \frac{\varepsilon_2}{4}\left[U_{11} - U_{11*}\right]. \quad (40)$$

If (40) is now substituted into the first term on the right-hand side of (37), the resulting contribution to the drift $\overline{U}^{(1)}$, say, may be expressed as

$$\frac{K_0}{2}\frac{d\overline{U^{(1)}}}{dz} = \frac{i\omega}{2c}\left[U_{11*}\int_0^z U_{11}dz - U_{\infty 1*}\int_0^\infty U_{11}dz\right]\left[1 + \frac{1}{4}(\varepsilon_2 + \varepsilon_{2*})\right] \quad (41)$$

from which, recalling that $\varepsilon_2 = |\varepsilon_2|\exp(i\varphi_2)$, it follows that

$$\overline{U^{(1)}} = \overline{U_s}\left[1 + \tfrac{1}{2}|\varepsilon_2|\cos\varphi_2\right]. \quad (42)$$

No terms of order ε_2^2 arise in (42).

In obtaining (21) for U_1, we treated ε_2 as a small parameter and then, in the appendix, showed how the solution is affected if ε_2 is not small (i.e., if terms of order ε_2^2 are retained in the analysis). If this assumption is also made in the determination of the Eulerian drift and (A7) is used instead of (21), the final result for the drift arising from term 1 on the right-hand side of (37) differs from (42) in two respects; first, the shear wavenumber α is replaced by β as defined by (A6) and, second, the coefficient in (42) $[1 + \tfrac{1}{2}|\varepsilon_2|\cos\varphi_2]$ is replaced by

$$\frac{2 + |\varepsilon_2|\cos\varphi_2}{\sqrt{4 - |\varepsilon_2|^2}}. \quad (43)$$

The modified drift profile, which is stated in the appendix as (A8), is correct to order ε_2^2. The effects of the two modifications to (42) are, first, that the vertical decay rate in the solution becomes rather greater (since $\beta > \alpha$) and, second, that the magnitude of the drift also becomes greater since

$$(1 + \tfrac{1}{2}|\varepsilon_2|\cos\varphi_2)\ (1 - \tfrac{1}{4}|\varepsilon_2|^2)^{-1/2} \sim 1 + \frac{|\varepsilon_2|}{2}\cos\varphi_2 + \frac{|\varepsilon_2|^2}{8} + \ldots. \quad (44)$$

4.1.2. Term 2. The first of the two asymmetry terms in (37) is readily evaluated to give the second contribution to the drift, $\overline{U}^{(2)}$. Substitution of (18) into the second term on the right-hand side of (37) yields

$$\frac{d\overline{U^{(2)}}}{dz} = -\tfrac{1}{2}\varepsilon_1 U_0\alpha(1-i)e^{-\alpha(1-i)z}, \quad (45)$$

and integration of this with respect to z, subject to the no-slip condition at $z = 0$, gives

$$\overline{U^{(2)}} = \tfrac{1}{2}U_0|\varepsilon_1|\left[e^{-\alpha z}\cos(\alpha z + \varphi_1) - \cos\varphi_1\right], \quad (46)$$

where $\varepsilon_1 = |\varepsilon_1|\exp(i\varphi_1)$. This solution, being derived from U_{11} (equation (18)) rather than U_1 (equation (21)) neglects terms involving the product $(\varepsilon_1\varepsilon_2)$ and so is consistent with the perturbation procedure. However, if $(\varepsilon_1\varepsilon_2)$ terms are included on the grounds that term 2 is only $O(kA_0)$ (see Table 1) and also that either ε_1 or ε_2 may not be small, then the solution based upon (21) becomes

$$\overline{U^{(2)}}|_m = -U_0\frac{|\varepsilon_1|}{2}\left\{\cos\varphi_1 - e^{-\alpha z}\left[\cos(\alpha z + \varphi_1) - \frac{|\varepsilon_2|}{2}\sin(\varphi_1 - \varphi_2)\sin\alpha z\right]\right\}. \quad (47)$$

However, in practice, the effect of the extra $\varepsilon_1\varepsilon_2$ term has been found to be very small, supporting the present perturbation approach.

4.1.3. Term 3. The second of the two asymmetry terms in (37) yields the third and final contribution to the drift, $\overline{U}^{(3)}$. If U_{21} given by (30) is substituted into the third term on the right-hand side of (37) and the no-slip condition is again applied at $z = 0$, it may be shown that $\overline{U}^{(3)}$ is given by

$$\overline{U^{(3)}} = \frac{|\varepsilon_2| U_0^2}{4c}\left\{e^{-\alpha z}\cos(\alpha z + \varphi_2) + \alpha z e^{-\alpha z}\left[\cos(\alpha z + \varphi_2) + \sin(\alpha z + \varphi_2)\right] - e^{-\sqrt{2}\alpha z}\cos(\sqrt{2}\alpha z + \varphi_2)\right\} + \frac{|\varepsilon_2|}{2} B U_0\left[e^{-\sqrt{2}\alpha z}\cos(\sqrt{2}\alpha z + \varphi_2) - \cos\varphi_2\right]. \quad (48)$$

This solution, being derived from U_{21} (equation (30)), neglects square terms $O(\varepsilon_2^2)$, as well as the $\varepsilon_1\varepsilon_2$ term that would have arisen from the inclusion in (26) of the ε_1 term in the second-order stress field. However, the present approach is a consistent one, since term 3 is $O(kA_0)^2$. The final solution for the drift is obtained from the sum of the three terms given by (42), (46), and (48):

$$\overline{U} = \overline{U^{(1)}} + \overline{U^{(2)}} + \overline{U^{(3)}}. \quad (49)$$

If these terms are evaluated at the edge of the boundary layer, the expression for the drift becomes simply

$$\overline{U_\infty} = \overline{U_\infty^{(1)}} + \overline{U_\infty^{(2)}} + \overline{U_\infty^{(3)}} = \overline{U_{\infty s}}\left[1 + \tfrac{1}{2}|\varepsilon_2|\cos\varphi_2\right] - \tfrac{1}{2}U_0|\varepsilon_1|\cos\varphi_1 - \tfrac{1}{2}U_0|\varepsilon_2| B\cos\varphi_2, \quad (50)$$

in which $\overline{U}_{\infty s} = \frac{3}{4}U_0^2/c$.

4.2. Model Predictions for the Eulerian Drift

The model prediction for the nondimensional Eulerian drift ($\overline{U}_\infty c/U_0^2$) for a representative asymmetrical wave is shown in Figure 1, together with the classical drift profile of *Longuet-Higgins* [1958] (hereinafter referred to as LH) (equation (39)). The parameter settings, which are typical of those determined for the experimental data sets in section 5, are as follows: asymmetry parameter $B = 0.1$ and propagation parameter $c/U_0 = 10$. This value of c/U_0 is physically reasonable since $c/U_0 = (A_0k)^{-1}$ and (A_0k) was treated earlier as a small paramcter. The phase angles φ_1 and φ_2 are defined according to (54) (see section 5.2.1), such that the dominant eddy viscosity peak during the wave cycle occurs at the instant of flow reversal following the passage of the wave crest (here $\varphi_1 = -80°$). The values of $|\varepsilon_1|$ and $|\varepsilon_2|$ have both been taken as 1.3. The use of such large values was justified earlier with reference to the comparison made by DV97 with a solution obtained by the method of normal modes. However, it still may be considered disturbing that our data analysis (section 5) yields values of $|\varepsilon_1|$ and $|\varepsilon_2|$ greater than unity, implying a (slightly) negative eddy viscosity at certain instants in the wave cycle. In the first place, it should be noted that since we are considering a perturbation solution, no mathematical difficulty (i.e., singularity) arises when the sign of K changes. Further, the significance of the negative eddy viscosity should not be overstated. If a more complete model of the eddy viscosity had been adopted, including, for example, a fourth harmonic component in K with its positive peak values at the same instants as those of the second harmonic, negative values of K would not necessarily have arisen. This point is discussed more fully in section 6.

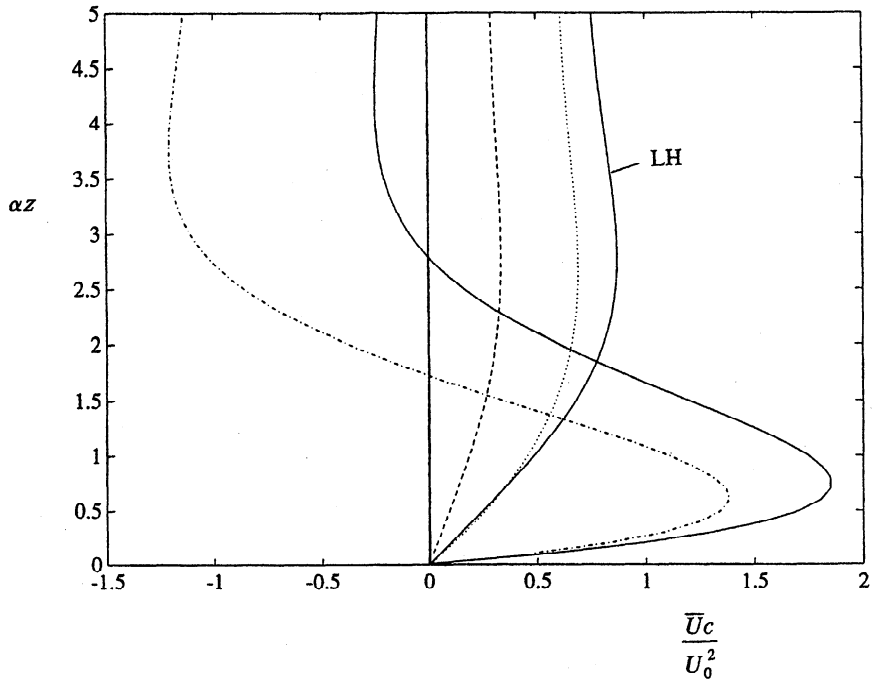

Figure 1. Representative spatially averaged drift profile resulting from asymmetrical waves above a very rough or rippled bed. The present model prediction $\overline{U}$ (equation (49)) is shown by the solid line, and its component parts $\overline{U}^{(1)}$, $\overline{U}^{(2)}$ and $\overline{U}^{(3)}$ by the dashed, dash-dotted, and dotted lines, respectively. Parameter settings are $B = 0.1$; $c/U_0 = 10$, where c is wave speed and U_0 is near-bed velocity amplitude; with $|\varepsilon_1| = |\varepsilon_2| = 1.3$. Phase angles φ_1 and φ_2 are given by (55); here $\varphi_1 = -80°$. *Longuet-Higgins'* [1953] solution (solid line labelled LH) is shown for comparison.

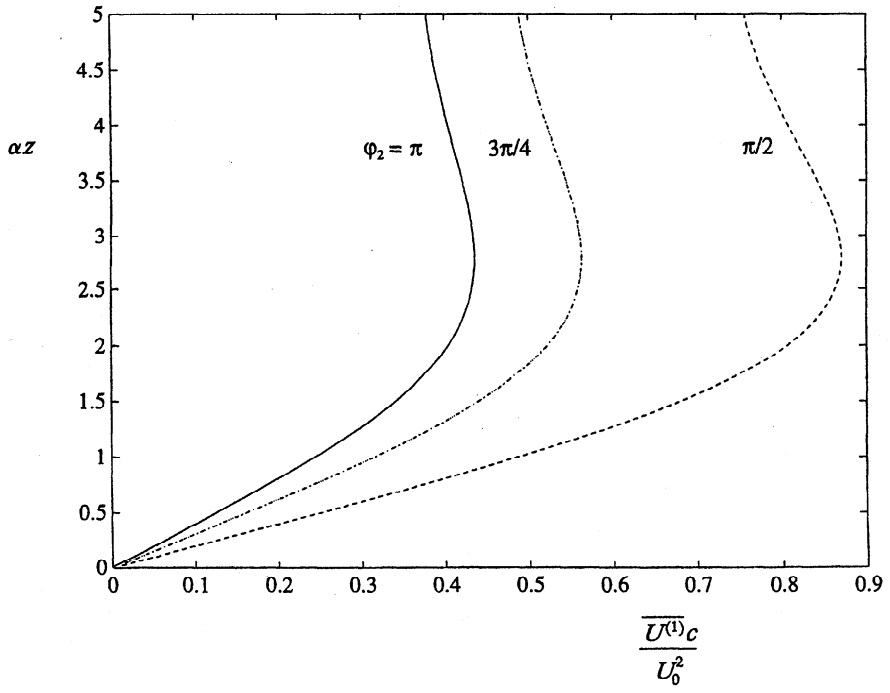

Figure 2a. Profiles of drift component $\overline{U}^{(1)}$ with $|\varepsilon_2| = 1$ and $\varphi_2 = \pi/2$ (dashed line), $3\pi/4$ (and $5\pi/4$) (dash-dotted line), and π (solid line).

In Figure 1 the drift profile given by (49) is shown by the solid line, and the contributions of terms 1, 2 and 3 (equations (42), (46), and (48)) are shown by the dashed, dash-dotted, and dotted lines, respectively. In comparison with LH (labeled solid line), the direction of the Eulerian drift is reversed at the edge of the boundary layer. Here positive contributions from terms 1 and 3 are offset by a large negative contribution from term 2. This latter effect is predicted also by *Trowbridge and Madsen*'s [1984b] eddy viscosity model for long (asymmetrical) waves. In contrast, close to the bed, terms 1, 2, and 3 complement one another and the drift profile shows a pronounced forward jet, the reversal of the direction of drift occurring within the boundary layer (at $\alpha z = 2.8$). This effect is not predicted by Trowbridge and Madsen's model.

The predictions for the drift are dependent upon the values assumed for the complex coefficients ε_1 and ε_2, as well as on

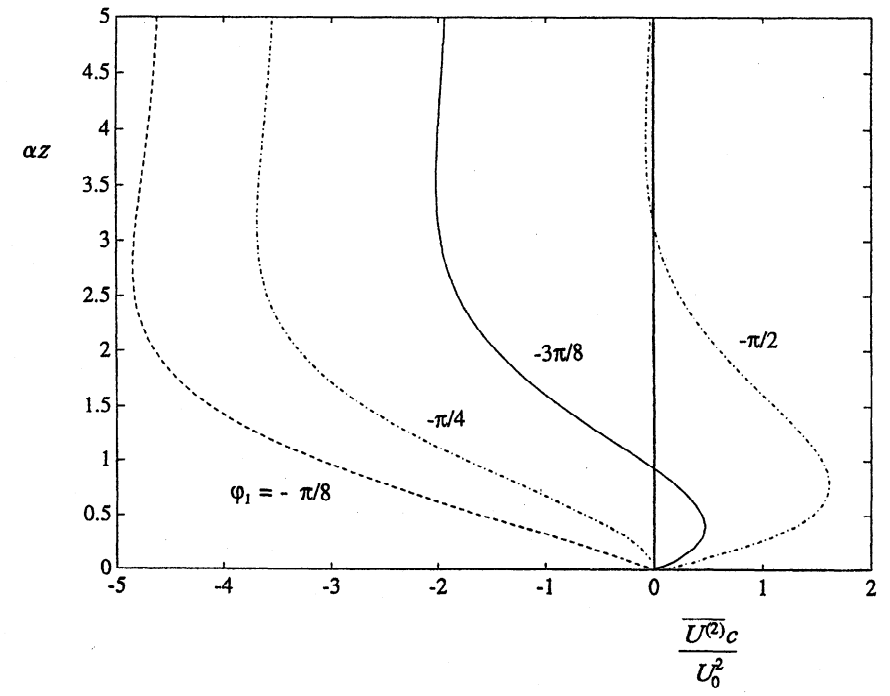

Figure 2b. Profiles of drift component $\overline{U}^{(2)}$ with $|\varepsilon_1| = 1$ and $\varphi_1 = -\pi/2$ (dotted line), $-3\pi/8$ (solid line), $-\pi/4$ (dash-dotted line), and $-\pi/8$ (dashed line).

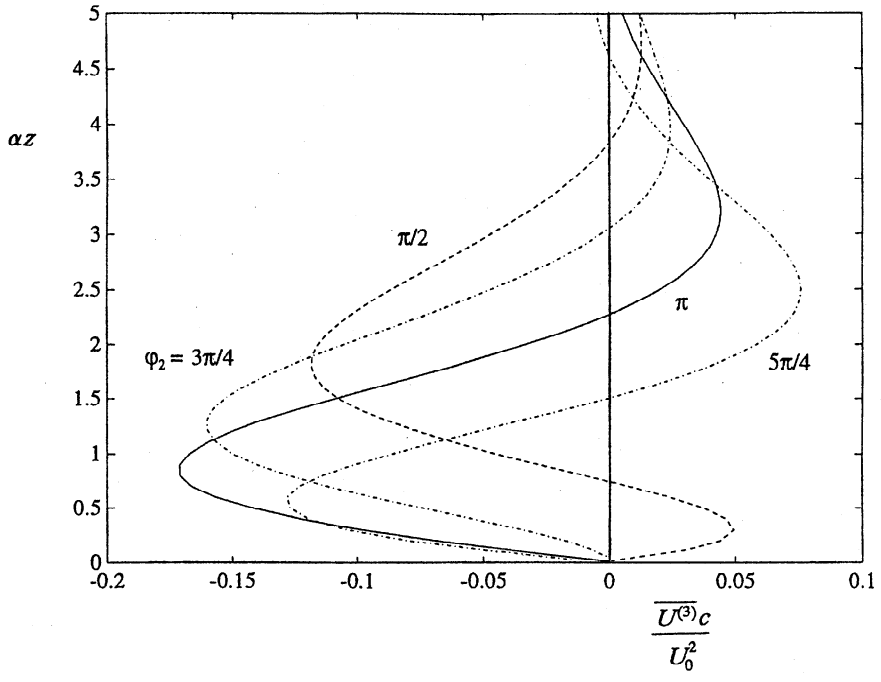

Figure 2c. Profiles of drift component $\overline{U}^{(3)}$ with $B = 0$, $c/U_0 = 10$, $|\varepsilon_2| = 1$, and $\varphi_2 = \pi/2$ (dashed line), $3\pi/4$ (dash-dotted line), π (solid line), and $5\pi/4$ (dotted line).

the values of the parameters B and c/U_0. First, the $\overline{U}^{(1)}$ contribution to the drift (equation (42)) depends upon the values of $|\varepsilon_2|$ and φ_2. The effect on $\overline{U}^{(1)}$ of varying φ_2 with $|\varepsilon_2| = 1$ is shown in Figure 2a, in which $\varphi_2 = \pi/2$ (dashed line) corresponds to LH; here the largest reduction in the drift is given by $\varphi_2 = \pi$ (solid line). Second, the $\overline{U}^{(2)}$ contribution (equation (46)) depends upon $|\varepsilon_1|$ and φ_1. The effect on $\overline{U}^{(2)}$ of varying φ_1 with $|\varepsilon_1| = 1$ is shown in Figure 2b. The essential difference between the predictions of the present convective eddy viscosity model and *Trowbridge and Madsen*'s [1984b] model lies in the behavior of this (dominant) $\overline{U}^{(2)}$ term. Above very rough and rippled beds, flow reversal occurs such that $\overline{U}^{(2)}$ has the form of the profile for $\varphi_1 = -3\pi/8$ in Figure 2b. In contrast, Trowbridge and Madsen's solution for less rough beds corresponds to values of φ_1 in the range $\pi/10$ to $\pi/5$. Thus, in the former case, there is a forward near-bed jet with a backward drift in the outer boundary layer, while, in the latter case, the drift is in the backward direction at all heights.

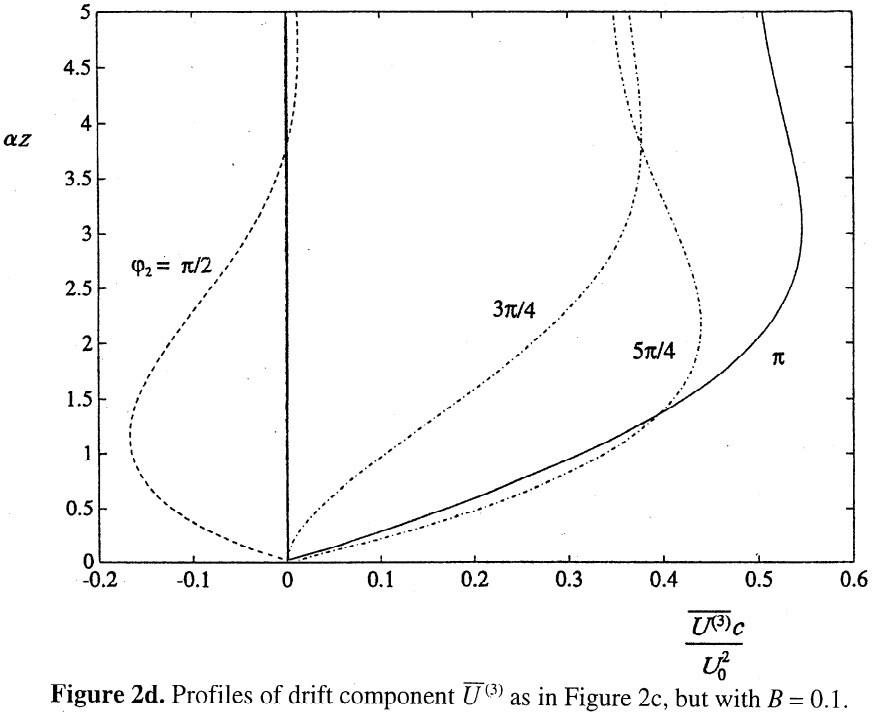

Figure 2d. Profiles of drift component $\overline{U}^{(3)}$ as in Figure 2c, but with $B = 0.1$.

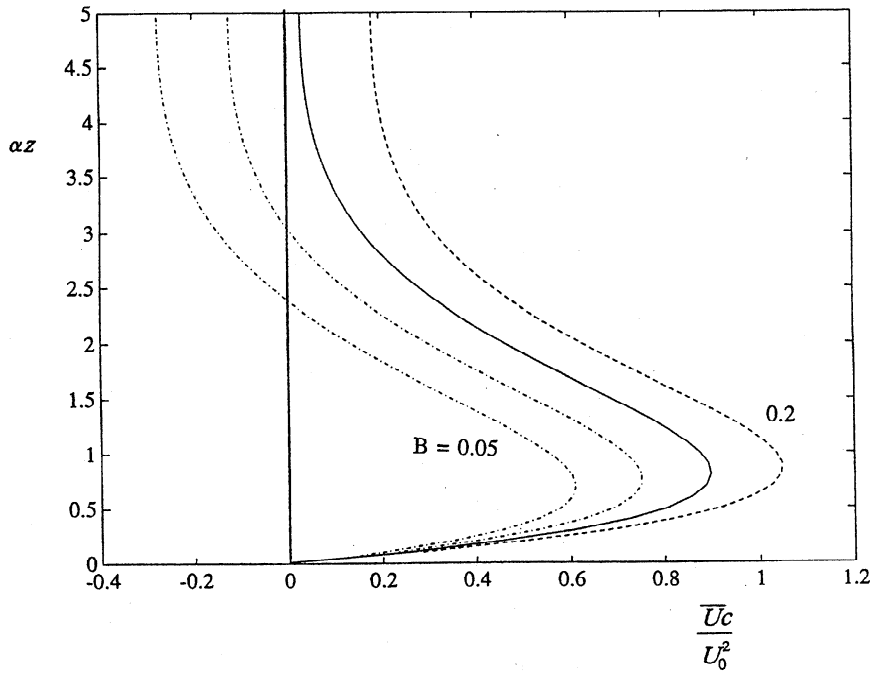

Figure 3a. Drift profiles for asymmetrical waves each having the values of $|\varepsilon_1|$, φ_1, $|\varepsilon_2|$, and φ_2 used in Figure 1, with $c/U_0 = 10$ and $B = 0.05$ (dotted line), 0.1 (dash-dotted line), 0.15 (solid line), and 0.2 (dashed line).

Finally, the $\overline{U}^{(3)}$ contribution (equation (48)) depends not only upon $|\varepsilon_2|$ and φ_2 but also on the values of the parameters B and c/U_0. Figure 2c shows the effect on $\overline{U}^{(3)}$ of varying φ_2, with $|\varepsilon_2| = 1$, $B = 0$, and $c/U_0 = 10$. Figure 2d shows the same profiles but now with $B = 0.1$; the change in the value of B increases the magnitude of this contribution and produces a nonzero value at the edge of the boundary layer.

The results shown in Figure 1 are sensitive to the values of the parameters B and c/U_0. This is highlighted in Figure 3a, where the effect of increasing the asymmetry parameter B while keeping c/U_0 constant is to increase both the near-bed jet and the (negative) outer flow drift. In Figure 3b, the effect of increasing c/U_0, while keeping B constant, is to increase the magnitude of the mean velocity gradient; the near-bed maximum drift is increased, while the outer flow drift is decreased.

In section 5 the present model results for the Eulerian drift are compared with various published data sets. For brevity, we have not included examples of profiles of velocity amplitude and phase (first and second harmonics). For such comparisons, the reader is referred to DV97.

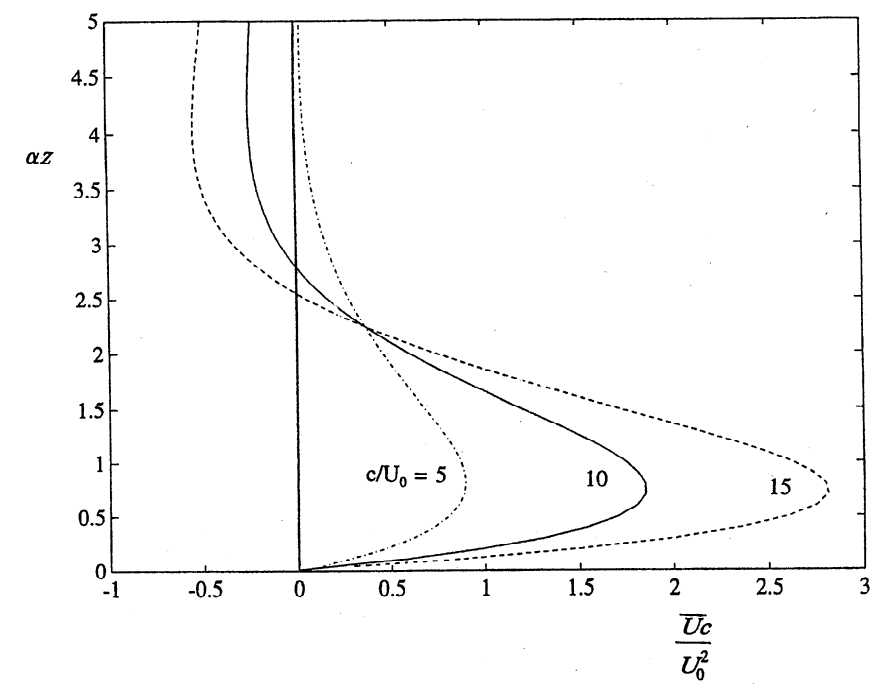

Figure 3b. Same as Figure 3a, but for $B = 0.1$ and $c/U_0 = 5$ (dash-dotted line), 10 (solid line), and 15 (dashed line).

5. Comparisons Between Measurements of Eulerian Drift and Model Predictions

5.1. Laboratory Data Sets

We consider five laboratory studies of the Eulerian drift in the bottom boundary layer beneath progressive waves. The relevant aspects of these studies, the first four of which were considered by DV98, are summarized below. For full details of the experimental conditions, the original papers (cited below) should be consulted. We make comparisons here only with the subset of tests carried out in the rough turbulent regime, the details of which are given in Tables 2 and 3. Unless stated otherwise, vertical profiles of velocity were measured in the respective tests using an LDA system. In several cases, these profiles include not only the bottom wave boundary layer but also a significant region of the "interior" flow above this.

5.1.1. *Van Doorn and Godefroy* [1978]. A flume experiment (tests RA/RB) was carried out with waves alone, above a bed comprising 2-D strip roughness (of height 0.2 cm) distributed over a 1.5 m test section. The velocity profiles were measured above the roughness crests and troughs. The equivalent bed roughness, taken here as k_s = 2.1 cm, was obtained from a logarithmic fit to a mean velocity profile measured in steady flow conditions.

5.1.2. *Sleath* [1984]. Flume experiments were carried out using a single layer of gravel of median diameter D = 1.1 cm, distributed uniformly over the bed for a distance of 8 m. In this case, no vertical profiles of velocity were obtained and the results reported were of the maximum near-bed drift, rather than the drift at the edge of the boundary layer. In addition, the results were spatially averaged across the width of the flume. Following *Sleath* [1984], we have taken the bed roughness as $k_s = 2D_{90}$ = 2.45 cm.

5.1.3. *Villaret and Perrier* [1992] [see also *Villaret and Latteux*, 1992]. Three experiments were carried out with progressive waves above a test section of 20 m length comprising mobile, rippled sand (D = 0.009 cm). Of these, tests 35 and 39 are considered to be the best, since lateral reflections and free waves may have affected the results in the remaining case. The spatially averaged horizontal velocity was measured with a 1-D ultrasonic meter, and the drift values reported here were recorded at levels uncontaminated by suspended sediment. While the equilibrium profiles were reasonably symmetrical, the ripple pattern was transitional between two and three dimensional. In test 39, the representative ripple height η was 0.75 cm and the wavelength λ was 6.1 cm; the equivalent bed roughness given by *Swart*'s [1976] formula (see below) was therefore k_s = 2.31 cm.

5.1.4. *Marin and Sleath* [1994]. Three experiments were carried out in a 17.5 m flume, above a test section comprising a fixed, stabilized sand bed of symmetrical 2-D ripples. The ripple height η was 0.8 cm, and wavelength λ was 4.5 cm; the equivalent roughness was therefore k_s = 3.6 cm. Since Eulerian drift profiles were measured only very close to the bed (in a layer of thickness about $\lambda/5$) at both crests and troughs, the appropriate basis for comparison with the other data and also with our model is less clear in this case.

5.1.5. *Mathisen and Madsen* [1996a, b]. Nine experiments were carried out in a 28 m flume above a test section comprising transverse 2-D triangular bars of height 1.5 cm and spacing 10 cm (20 cm in some cases). Eulerian drift profiles were measured above both crests and troughs of the bars. Representative equivalent roughness values were determined from

Table 2. Hydrodynamic Parameter Settings Used in the Laboratory Experiments

Test	Period T, s	Depth h, m	Wave Height H, m	U_0, m s^{-1}	kh	B	c/U_0
MS1	1.35	0.2	0.029	(0.080)	0.72	(0.10)	(16.2)
				0.086		0.08	15.0
MS2	1.38	0.2	0.048	(0.121)	0.70	(0.17)	(10.8)
				0.144		0.15	9.0
MS3	1.33	0.2	0.064	(0.158)	0.73	(0.15)	(8.2)
				0.190		0.17	6.8
MMa	2.24	0.6	0.101	0.171	0.75	0.084	13.0
MMb	2.63	0.6	0.107	0.190	0.63	0.139	12.0
MMc	2.89	0.6	0.106	0.193	0.57	0.177	12.0
MMd	2.24	0.6	0.070	0.118	0.75	0.058	18.9
MMe	2.63	0.6	0.077	0.137	0.63	0.100	16.7
MMf	2.89	0.6	0.074	0.136	0.57	0.124	17.0
MMm	2.24	0.6	0.099	0.167	0.75	0.082	13.3
MMn	2.63	0.6	0.107	0.191	0.63	0.140	11.9
MMo	2.89	0.6	0.110	0.200	0.57	0.183	11.6
VP35	1.50	0.6	0.232	0.300	1.26	0.040	6.7
VP39	2.00	0.6	0.232	0.373	0.86	0.135	5.8
VD RA/RB	2.00	0.3	0.120	(0.298)	0.58	(0.22)	(5.5)
				0.308		0.38	5.3
S11	1.92	0.334	0.085	0.202	0.64	0.19	8.4
S12	1.90	0.333	0.077	0.183	0.65	0.17	9.3
S13	1.86	0.333	0.073	0.172	0.67	0.15	11.3
S14	1.92	0.333	0.092	0.219	0.64	0.20	7.8
S28	0.96	0.193	0.085	0.217	1.07	0.08	5.5

Values were calculated using linear wave theory. Numbers in parentheses are measured values. Parameters are U_0, near-bed velocity amplitude; k, surface wavenumber; B, asymmetry parameter (see (29)); and c, wave phase speed. Test abbreviations are defined as follows: MS, *Marin and Sleath* [1994], tests 1-3; MM, *Mathisen and Madsen* [1996b], tests a-f and m-o; VP, *Villaret and Perrier* [1992], tests 35 and 39; VD, *Van Doorn and Godefroy* [1978], test RA/RB; and S, *Sleath* [1984], tests 11-14 and 28.

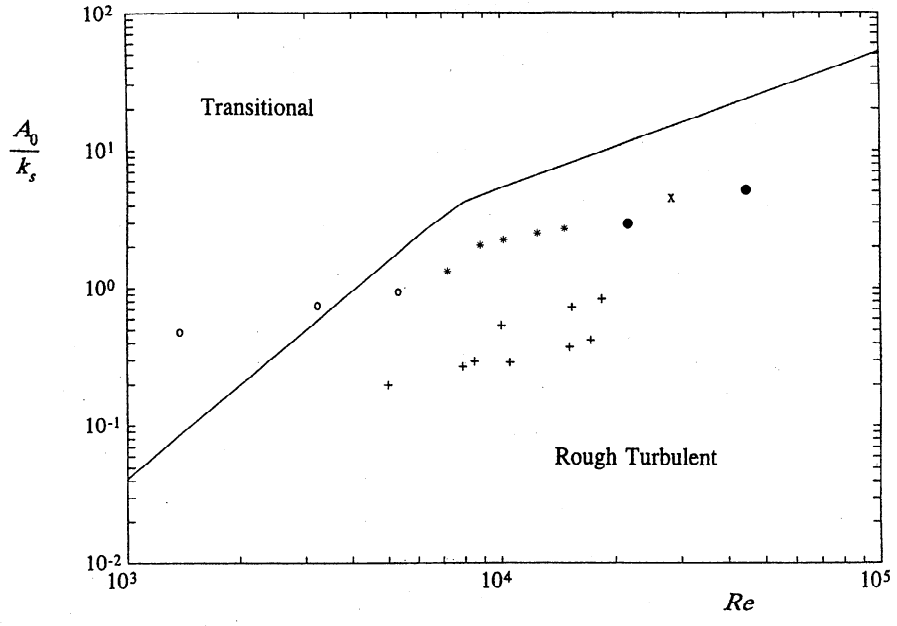

Figure 4. Delineation of flow regimes, indicating the boundary between transitional and very rough turbulent oscillatory flow. The symbols representing the data sets are as follows: asterisks, *Sleath* [1984]; open circles, *Marin and Sleath* [1994]; solid circles, *Villaret and Perrier* [1992]; pluses, *Mathisen and Madsen* [1996a,b]; and cross, *Van Doorn and Godefroy* [1978].

experiments involving currents alone, waves alone, and also combined wave and current flows, as $k_s = 21.3$ cm for the 10 cm bar spacing and $k_s = 11.1$ cm for the 20 cm spacing.

It should be noted that beach reflection was of negligible importance in each of these studies. In the experiments of *Van Doorn and Godefroy* [1978], the reflection coefficient R was zero due to the short duration of the tests [see also *Trowbridge and Madsen,* 1984b]. In the experiments of *Sleath* [1984], R was always less than 0.03, and since *Marin and Sleath*'s [1994] experiments were carried out with the same wave flume and beach, the same value of R may be inferred. In the tests of *Villaret and Perrier* [1992], R was about 0.05, and so beach reflection would not have appreciably affected the drift results. Although no value of R is quoted by *Mathisen and Madsen* [1996a, b], their discussion indicates that care was taken to ensure that the waves were of pure progressive type.

In discussing the respective data sets, we treat in exactly the same way the cases of rough (3-D) and rippled (2-D) beds. Initially, in Figure 4, we show the location of the various data points on the delineation of the $(Re, A_0/k_s)$ plane adopted by DV97, where the wave Reynolds number $Re = U_0 A_0/\nu$ (ν is kinematic viscosity). All of the data (except for two of *Marin and Sleath*'s [1994] tests) lie in the very rough turbulent regime. Linear theory has been used here to calculate the wave parameters (U_0, A_0, etc.) from the measured water depth h, wave height H, and angular frequency ω in each test. Where an equivalent roughness has been determined experimentally, this has been used in the classification (see Table 3). Otherwise, for the two cases involving ripples, *Swart*'s [1976] formula has been used, namely, $k_s = 25\eta(\eta/\lambda)$. It may be noted that if the values determined experimentally for k_s in the experiments of *Van Doorn and Godefroy* [1978] and *Mathisen and Madsen* [1996a, b] are related in this way to the height and wavelength of the respective (sharp crested) roughness elements, it turns out that $k_s \approx 80\eta(\eta/\lambda)$. This suggests that the equivalent roughness may have been underestimated for the rippled beds by our use of Swart's formula, the shape as well as the size of the roughness elements evidently having a significant influence upon k_s.

The uncertainty in our determination of k_s is illustrated by the fact that the value A_0/k_s given for *Van Doorn and Godefroy*'s [1978] test RA/RB is comparable with that obtained for *Villaret and Perrier*'s [1992] test 39, despite the fact that, in the former case, the particle excursion amplitude A_0 corresponds to about six roughness spacings and, in the latter case, to only about one and a half ripple wavelengths. Although according to the value of A_0/k_s, the two cases are hydraulically equivalent, the conditions in test RA/RB are likely to have been influenced to a greater extent by turbulence and to a lesser extent by organized vortex shedding than in test 39. Thus a less strongly time varying eddy viscosity may be expected in the former case than in the latter (see section 6).

For a true comparison with the model, the Eulerian drift data should represent an appropriately averaged mean velocity, i.e., a horizontal average on at least the scale of the bed roughness elements. In practice, only *Sleath* [1984] presented his data in this form. In the experiments of *Villaret and Perrier* [1992], the measuring length scale was somewhat smaller than the ripple length. In the remaining experiments, LDA measurements were carried out above the crests and troughs of the bed roughness elements. In these cases, the Eulerian drift can be defined with confidence only if measurements made at the same absolute level at these two locations are reasonably consistent. Fortunately, in most of the experimental tests, this was the case. However, in the experiments of *Marin and Sleath* [1994], the data were obtained so close to the bed that most of the measurement levels in the trough were actually below the crest level.

An additional point relating to the basis for comparison between the present theory and the data sets above concerns the validity of the assumption (see (32)) that the mean bed

Table 3. Bed Roughness, Mean Eddy Viscosity $\frac{1}{2}K_0$ and Boundary Layer Thickness δ for the Experiments

Test	Roughness Type	Roughness Size, cm	k_s, cm	A_0/k_s	$\frac{1}{2}K_0$, $cm^2\ s^{-1}$	δ_s ($=\alpha^{-1}$), cm	δ_w, cm
MS1	2-D stabilized sand, rippled bed	$\lambda = 4.5$, $\eta = 0.8$	3.6	(0.48) 0.52	(0.11) 0.12	(0.22) 0.23	(1.1) 1.15
MS2	2-D stabilized sand, rippled bed	$\lambda = 4.5$, $\eta = 0.8$	3.6	(0.75) 0.89	(0.17) 0.21	(0.27) 0.30	(1.4) 1.5
MS3	2-D stabilized sand, rippled bed	$\lambda = 4.5$, $\eta = 0.8$	3.6	(0.94) 1.13	(0.22) 0.27	(0.31) 0.34	(1.5) 1.7
MMa	2-D triangular roughness elements	$\lambda = 10$, $\eta = 1.5$	21.3[a]	0.29	1.46	1.02	5.1
MMb	2-D triangular roughness elements	$\lambda = 10$, $\eta = 1.5$	21.3[a]	0.37	1.62	1.16	5.8
MMc	2-D triangular roughness elements	$\lambda = 10$, $\eta = 1.5$	21.3[a]	0.42	1.65	1.23	6.2
MMd	2-D triangular roughness elements	$\lambda = 10$, $\eta = 1.5$	21.3[a]	0.20	1.006	0.85	4.2
MMe	2-D triangular roughness elements	$\lambda = 10$, $\eta = 1.5$	21.3[a]	0.27	1.17	0.99	4.9
MMf	2-D triangular roughness elements	$\lambda = 10$, $\eta = 1.5$	21.3[a]	0.29	1.15	1.0	5.1
MMm	2-D triangular roughness elements	$\lambda = 20$, $\eta = 1.5$	11.1	0.54	0.74	0.73	3.6
MMn	2-D triangular roughness elements	$\lambda = 20$, $\eta = 1.5$	11.1	0.72	0.85	0.84	4.2
MMo	2-D triangular roughness elements	$\lambda = 20$, $\eta = 1.5$	11.1	0.83	0.88	0.90	4.5
VP35	rippled bed, 2-D (2½-D)	$\lambda = 5$, $\eta = 0.7$	2.45[a]	2.9	0.32	0.39	1.9
VP39	rippled bed, 2-D (2½-D)	$\lambda = 6.1$, $\eta = 0.75$	2.31[a]	5.2	0.49	0.56	2.8
VD	2-D square	$\lambda = 1.5$, $\eta = 0.2$	2.1	(4.5)	(0.34)	(0.46)	(2.3)
RA/RB	roughness			4.7	0.35	0.47	2.4
S11	immobile gravel bed	$D_{90} = 1.22$	2.45	2.53	0.20	0.35	1.8
S12	immobile gravel bed	$D_{90} = 1.22$	2.45	2.24	0.18	0.33	1.7
S13	immobile gravel bed	$D_{90} = 1.22$	2.45	2.08	0.17	0.32	1.6
S14	immobile gravel bed	$D_{90} = 1.22$	2.45	2.73	0.22	0.36	1.9
S28	immobile gravel bed	$D_{90} = 1.22$	2.45	1.35	0.21	0.25	1.3

See Table 2 for test abbreviations. Here k_s is equivalent bed roughness and s and w subscripts are defined such that wave boundary layer thickness $\delta_w = 5\delta_s = 5(K_0/\omega)^{1/2}$ (see (55)); λ is wavelength, and η is ripple height. Values in parentheses have been obtained from measured values. Mean eddy viscosity is given by *Nielsen*'s [1992] formula for $A_0/k_s < 2.5$ and *Sleath*'s [1991] formula for $A_0/k_s > 2.5$.

[a] *Swart*'s [1976] formula was used ($k_s = 25\eta(\eta/\lambda)$).

shear stress is equal to the mean stress at the edge of the wave boundary layer given by the terms on the right-hand side of (6). In fact, the total mean stress is not equal to this latter Reynolds stress term owing to momentum flux contributions arising in the boundary layer from the effects of (1) surface wave amplitude dissipation and (2) any surface (mean) slope in the wave flume in question. Following arguments similar to those adopted by *Nielsen and You* [1996], we have carried out a control-volume analysis to assess the balance of forces within the wave boundary layer, though, for brevity, the details of this are not included here. Essentially, for wave dissipation rates such as those measured by *Mathisen and Madsen* [1996a] and with the edge of the boundary layer as defined by (55), the momentum flux contribution due to dissipation is, at most, 0.12 times the (dominant) wave Reynolds stress component at the edge of the boundary layer. As far as the surface slope contribution is concerned, even if a substantial mean slope of $O(10^{-5})$ is assumed, the contribution to the momentum flux is no more than about one half of that due to wave dissipation. So, even in the worst case in which the two above effects complement one another, it is reasonable to assume that the total stress is approximately equal to the wave Reynolds stress. In relation to surface slope effects, *Mathisen and Madsen* [1996b] carried out a test on the return currents in their flume, from which they concluded that the drift observed at the edge of the wave boundary layer was the result of processes within the boundary layer.

The approach adopted in sections 5.2 and 5.3 is to use the various data sets to evaluate the coefficient ε_1 defining the asymmetrical component of the time-varying eddy viscosity K (see (15)). Comparisons are then made between the model predictions and measurements of the drift at the edge of the wave boundary layer, as well as with vertical profiles of the drift. For consistency and simplicity in the treatment of all the data sets and also in the model comparisons, the origin of z has been assumed to be located at the level midway between crest and trough of the bed roughness elements. This definition was adopted also by *Ranasoma and Sleath* [1992].

5.2. The Drift at the Edge of the Boundary Layer

5.2.1. Model prediction. According to (50), the nondimensional drift at the outer edge of the wave boundary layer ($\overline{U}_\infty$) is a function of both B and c/U_0. This may be seen when (50) is written

$$\frac{\overline{U}_\infty c}{U_0^2} = \frac{3}{4}\left[1 + \frac{1}{2}|\varepsilon_2|\cos\varphi_2\right] - \frac{1}{2}\frac{c}{U_0}|\varepsilon_1|\cos\varphi_1 - \frac{1}{2}B\frac{c}{U_0}|\varepsilon_2|\cos\varphi_2 . \quad (51)$$

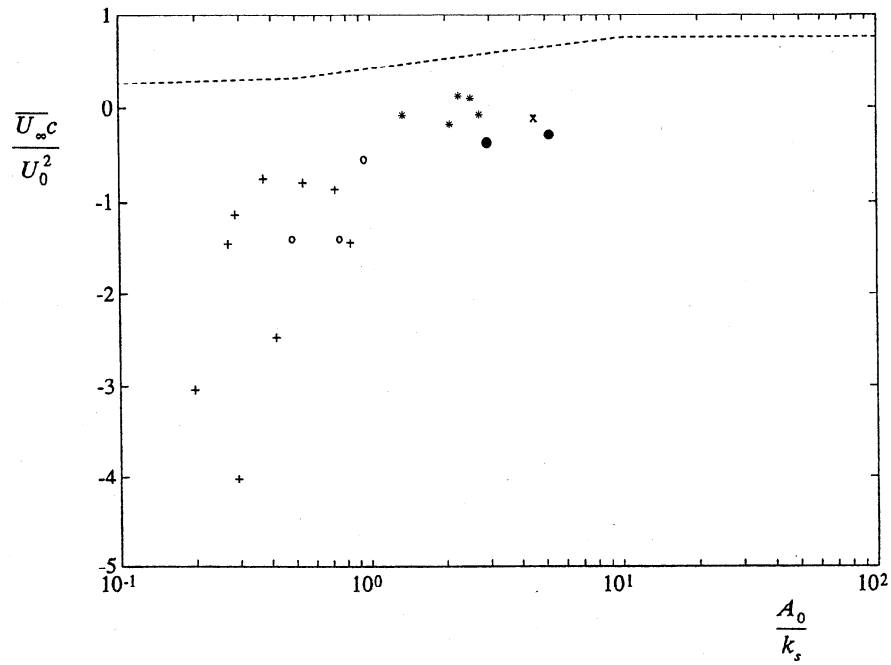

Figure 5. Nondimensional Eulerian drift at the edge of the boundary layer in relation to A_0/k_s. The dashed line shows the expected reduction (cf. *Longuet-Higgins*, 1953) in the drift for purely symmetrical waves, resulting from the behavior assumed for $|\varepsilon_2|$ by *Davies and Villaret* [1998]. The symbols representing the various data sets are as defined in Figure 4.

The first term on the right-hand side of (51) is the modification to the nondimensional drift (i.e., compared with the classical LH result of ¾) resulting from the time-varying viscosity for purely symmetrical waves. It was concluded by DV98 that this first term alone is insufficient to fully explain the reduction in the nondimensional drift observed in the very rough turbulent regime. This is shown in Figure 5, which also includes the recently published data of *Mathisen and Madsen* [1996b]. Here the dashed line represents the nondimensional drift determined by DV98 for purely symmetrical waves. It was assumed by DV98 that $|\varepsilon_2| = 1.3$ and $\varphi_2 = \pi$ for $A_0/k_s \le 1$ and $|\varepsilon_2| = 0$ for $A_0/k_s \ge 30$, with $|\varepsilon_2|$ decreasing linearly between these values in the range $1 < A_0/k_s < 30$.

The second and third terms on the right-hand side of (51) account for the effects of wave asymmetry. Since the product Bc/U_0 in the third term is equal to $3/[4\sinh^2 kh]$ (from (29)), (51) can be rewritten

$$\frac{\overline{U_\infty}c}{U_0^2} = \frac{3}{4}\left[1 + \frac{1}{2}\left(1 - \frac{1}{\sinh^2 kh}\right)|\varepsilon_2|\cos\varphi_2\right] - \frac{1}{2}\frac{c}{U_0}|\varepsilon_1|\cos\varphi_1 \ . \tag{52}$$

It follows that if both ε_2 and ε_1 remain approximately constant, the nondimensional drift should decrease linearly with increasing c/U_0, provided that kh is also approximately constant for the data considered. In the case of symmetrical waves it was established by DV97 that $\varphi_2 \approx \pi$, such that maxima in the time-varying eddy viscosity K occur at times of flow reversal. Here maxima in K are again linked to flow reversal in the wave cycle, but with the additional effects of wave asymmetry taken into account. If the free-stream flow, which includes both first and second harmonic components and also the residual velocity, is expressed as

$$U_\infty = U_0\left[\cos\omega t + B\cos 2\omega t + \frac{\overline{U_\infty}}{U_0}\right] \tag{53}$$

(see (33) in which we have taken $x = 0$, for convenience), then flow reversal following the passage of a wave crest occurs when $\omega t = \arccos\{B - \overline{U}_\infty/U_0\}$. Since eddy shedding is expected to occur slightly in advance of flow reversal, with phase lead $\Delta\varphi$, say [*Block et al*, 1994], we have defined the phase angle at which the principal peak in K occurs during the wave cycle, as follows:

$$\varphi_1 = -\arccos\left(B - \frac{\overline{U_\infty}}{U_0}\right) + \Delta\varphi \tag{54a}$$

with

$$\varphi_2 = 2\pi + 2\varphi_1 \ . \tag{54b}$$

These definitions have been used in all the comparisons below. For simplicity, we have used the measured values of $\overline{U}_\infty$ to obtain φ_1 from (54a) in the respective cases, which turns out to give consistent estimates for the drift.

5.2.2. Data sets. Most of the measured vertical profiles of Eulerian drift include not only the bottom wave boundary layer but also a significant region of the interior flow above this. Since, in practice, variations in the mean velocity occur near the edge of the boundary layer, a consistent definition of the boundary layer thickness is essential in the determination of the values of $\overline{U}_\infty$. Here we have defined the wave boundary layer thickness δ_w as

$$\delta_w = 5\delta_s \tag{55a}$$

where

$$\delta_s = \frac{1}{\alpha} = \sqrt{\frac{K_0}{\omega}} \tag{55b}$$

Table 4. Comparison of Laboratory Data and Standard Model of Eulerian Drift at the Edge of the Wave Boundary Layer, $z = z_\infty$

Test	Measurements of Vertical Profile of Drift		Measured Drift Velocity		Model Prediction
	Location	z_∞, cm	$\overline{U}_\sim$, cm s^{-1}	$\overline{U}_\sim$ c/U$_0^2$	$\overline{U}_\sim$ c/U$_0^2$
MS1	crest and trough	0.9	(-0.69)	(-1.4)	(-1.44)
			-0.81		-1.35
MS2	crest and trough	0.9	(-1.57)	(-1.4)	(-1.31)
			-2.22		-1.13
MS3	crest and trough	0.9	(-1.06)	(-0.55)	(-0.51)
			-1.53		-0.45
MMa	crest and trough	8.5	-1.5	-1.14	-1.08
MMb	crest and trough	5.25	-1.2	-0.76	-0.85
MMc	crest and trough	6.0	-4.0	-2.47	-2.19
MMd	none	5.25	-1.9	-3.04	-2.58
MMe	none	5.25	-1.2	-1.46	-1.50
MMf	none	5.25	-3.2	-4.02	-3.38
MMm	none	5.25	-1.0	-0.80	-0.87
MMn	none	5.25	-1.4	-0.87	-0.93
MMo	none	5.25	-2.5	-1.44	-1.42
VP35	spatial average	2.0	-1.60	-0.36	-0.25
VP39	spatial average	2.8	-1.80	-0.28	-0.18
VD RA/RB	crest and trough	2.3	-0.60	(-0.11)	(-0.11)
				-0.10	-0.37
S11	none	max. Eulerian drift	2.6	0.11	-0.10
S12	none	max. Eulerian drift	2.6	0.13	-0.12
S13	none	max. Eulerian drift	-3.0	-0.17	-0.34
S14	none	max. Eulerian drift	-1.8	-0.06	-0.21
S28	none	max. Eulerian drift	-2.7	-0.07	-0.02

For the standard model, see (51) in which $|\varepsilon_1|=|\varepsilon_2|=1.3$, with φ_1 and φ_2 given by (54) in which $\Delta\varphi=4°$. Values in parentheses have been obtained from measured values.

which, according to Stokes' solution (18), is approximately double the height at which the velocity maximum or "overshoot" occurs on the vertical profile of U_{11}. The cycle-mean value of the convective eddy viscosity ($\frac{1}{2}K_0$) (see (15)) has been estimated using the formula of either *Nielsen* [1992] or *Sleath* [1991], according to whether A_0/k_s is less than or greater than 2.5 (the value at which the two formulas are in agreement):

$$\frac{K_0}{2} = 0.004U_0k_s \qquad \frac{A_0}{k_s} < 2.5$$

$$\frac{K_0}{2} = 0.00253U_0k_s\sqrt{\frac{A_0}{k_s}} \qquad \frac{A_0}{k_s} > 2.5 \tag{56}$$

The values of $\frac{1}{2}K_0$, $1/\alpha$, and δ_w thus calculated for the various data sets are given in Table 3. For example, in the case of *Van Doorn and Godefroy*'s [1978] experiment, the edge of the boundary layer is given by (55) as $\delta_w \approx 2.4$ cm, which corresponds to approximately twice the height at which the maximum overshoot was observed. In tests 35 and 39 of *Villaret and Perrier* [1992], the values of δ_w given by (55) correspond to 2.7 and 3.7 times the ripple height, respectively.

The measured values of Eulerian drift estimated on this basis at the edge of the boundary layer are given in Table 4. In tests 35 and 39 of *Villaret and Perrier* [1992] and also in the experiments of *Van Doorn and Godefroy* [1978] (test RA/RB) and *Mathisen and Madsen* [1996a, b] (tests a, b, and c), measurements of the drift were made throughout the wave boundary layer. In these cases, the values of $\overline{U}_\infty$ have been obtained by interpolating the velocity measurements made near the edge of the boundary layer. In the case of Mathisen and Madsen's test a, the value calculated for δ_w is clearly an underestimate (by a factor about 1.8, as discussed later), and so here the outer flow drift has been obtained by interpolating the velocity data at a height of 9 cm, rather than at $\delta_w = 5.1$ cm. In Mathisen and Madsen's tests d to o, we have used the values of the Eulerian drift quoted by the authors, which were measured at a constant elevation of $z = 5.25$ cm, just above the boundary layer ($\delta_w = 3.6$ - 5.1 cm; see Table 3). In the experiments of *Marin and Sleath* [1994], drift velocities were measured only in a near-bed layer of thickness 0.9 cm. These measurements did not therefore extend to the edge of the boundary layer (δ_w = 1.1 to 1.5 cm); here we consider only the drift measured above the crest and have taken the uppermost measurement level (at height ≈ 9 mm) as the edge of the boundary layer (see Table 4). In the data sets of *Sleath* [1984], the measurements were of the maximum (averaged) drift within the boundary layer.

5.2.3. Estimates of model coefficients. In order to determine the parameters ε_1 and $\Delta\varphi$ in the time-varying eddy viscosity model, (52) has been compared with our estimates in Table 4 of the Eulerian drift. The measurements of non-dimensional Eulerian drift are plotted against $(c/U_0)\cos(\varphi_1)$ in Figure 6. According to (52), the value of $|\varepsilon_1|$ should be given by twice the slope of a best fit regression line. Here a standard linear regression procedure has been used to determine $|\varepsilon_1|$, while the phase lead $\Delta\varphi$ has been treated as a fitting parameter. The best fit line in Figure 6 corresponds to $|\varepsilon_1| = 1.3$ (±0.2 defining the 90% confidence interval) with $\Delta\varphi = 4°$.

These new results for $|\varepsilon_1|$ and $\Delta\varphi$, together with the previous estimate of $|\varepsilon_2| = 1.3$ used by DV98, are assumed initially to remain constant in a "standard" time-varying eddy

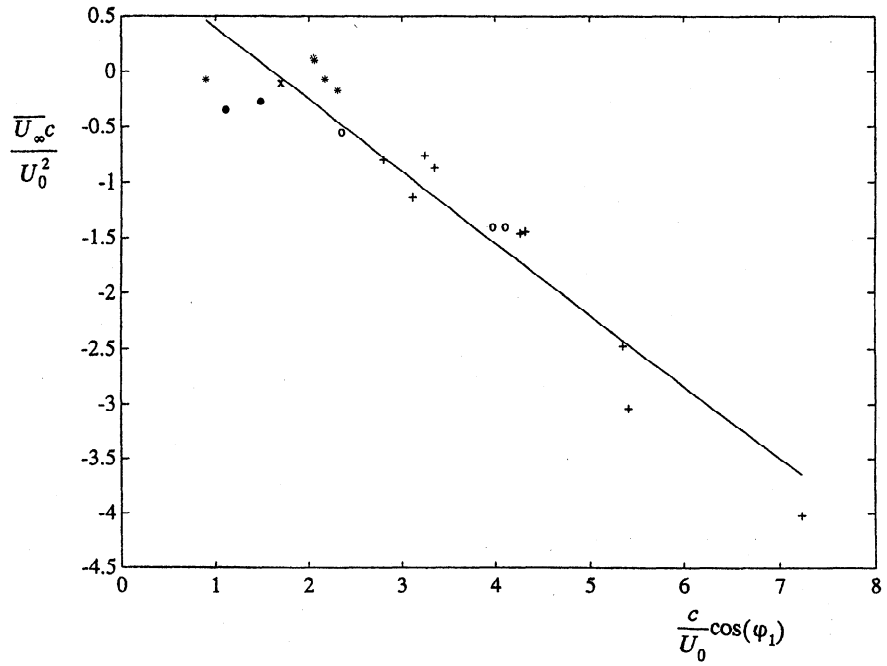

Figure 6. Nondimensional Eulerian drift in relation to $(c/U_0)\cos\varphi_1$. The symbols representing the various data sets are as defined in Figure 4. The best fit regression line corresponds to $|\varepsilon_1| = 1.3$ with $\Delta\varphi = 4°$.

viscosity model for the very rough turbulent regime. This global model for K, which applies to the parameter range corresponding to the present data sets, is illustrated in Figure 7. The dominant (first) peak in the nondimensional eddy viscosity $[K/(\frac{1}{2}K_0)]$ follows the passage of the steep wave crest, while the smaller (second) peak follows the trough. The relative magnitude of the two peaks is 3.6. The larger peak occurs 4° ahead of flow reversal, which corresponds to the expected phase lead of vortex ejection before reversal in the free stream.

The standard model has been used to predict the drift at the edge of the boundary layer for each data set. As noted in section 4.2, the model results are sensitive to the values of the coefficients B and c/U_0 defining the wave asymmetry. Both coefficients can be calculated using linear wave theory (see (12)), given the period, water depth, and (local) wave height. However, waves generated in flume experiments may be perturbed significantly by parasitic reflections and second-order free waves, such that the amplitudes (and phases) of the first and second harmonics of velocity may differ locally

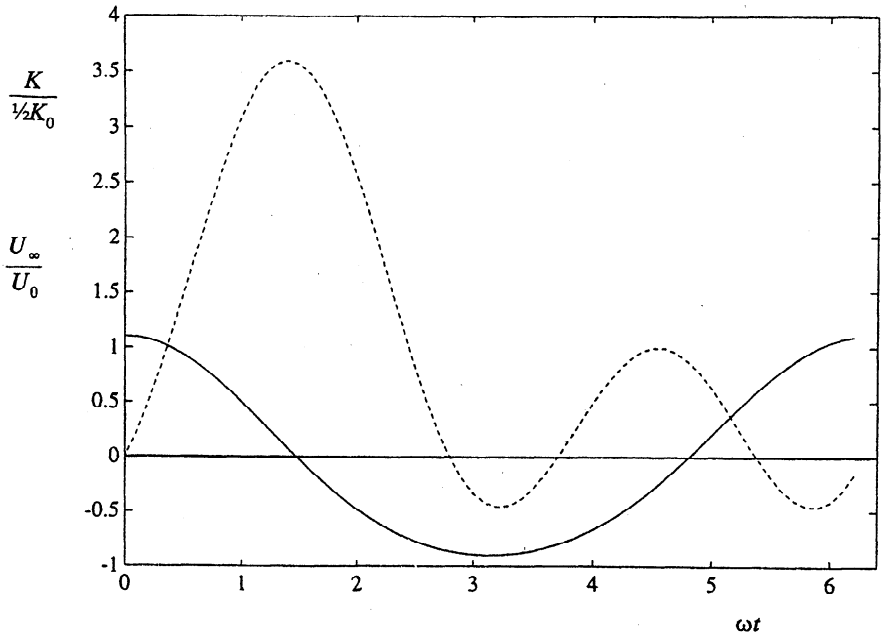

Figure 7. Standard time-varying eddy viscosity model for asymmetrical waves in the very rough turbulent regime. The solid line represents velocity variation through the wave cycle with $B = 0.1$, while the dashed line represents the nondimensional eddy viscosity $K/(\frac{1}{2}K_0)$.

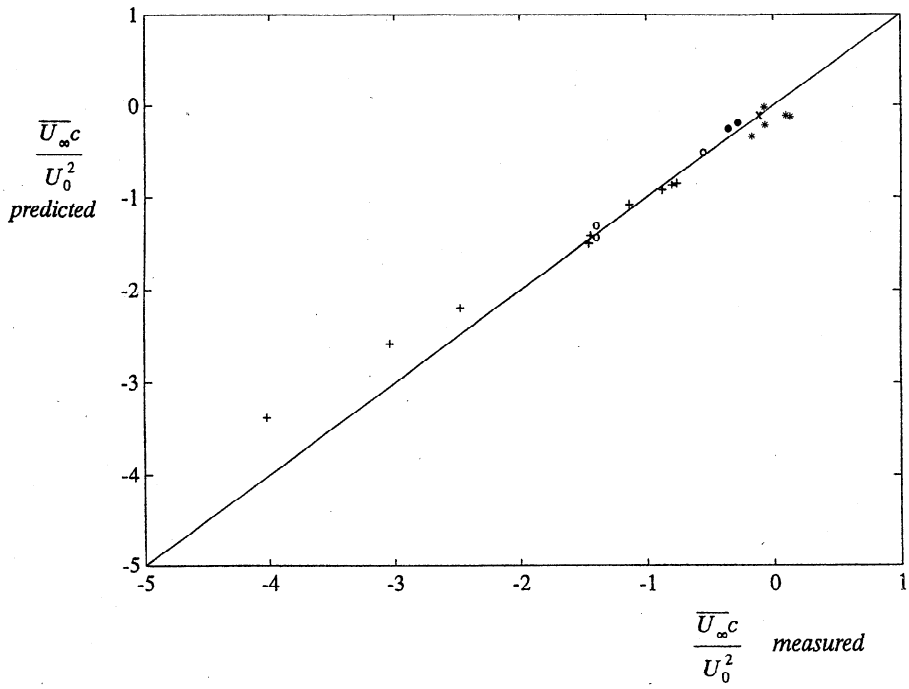

Figure 8. Comparison between the predicted and measured values of the nondimensional Eulerian drift at the edge of the boundary layer using the standard time-varying eddy viscosity model. Perfect agreement corresponds to the solid line. The symbols representing the various data sets are as defined in Figure 4.

from the theoretical values. In Table 2, the measured values of B and c/U_0 are shown (where available) in parentheses, while theoretically calculated values are shown without enclosures. The predictions of the outer flow Eulerian drift in Table 4 have been made using both the measured and theoretical values, the agreement with the data generally being improved by using the measured values.

The predictions of the standard model shown in Figure 8 are in good overall agreement with the data and certainly represent an improvement on the classical LH value (of ¾) for the nondimensional drift. In the case of *Sleath*'s [1984] data, the standard model suggests a rather stronger reversal in the drift than that which was observed. However, this is as expected since it was the maximum drift that was measured in this case, rather than the drift at the edge of the boundary layer. The model also tends to underestimate systematically the large (negative values of) drift reported in some of *Mathisen and Madsen*'s [1996b] data (tests c, d and f). This discrepancy could be due to a dependence of the eddy viscosity model coefficients (ε_1, ε_2, and $\Delta\varphi$) on the degree of wave asymmetry and also on the relative roughness (A_0/k_s). The effect of varying these parameters is discussed in section 6.

5.3. Model Predictions of Vertical Profiles of Eulerian Drift

For those tests where vertical profiles are available, the standard model ($|\varepsilon_1| = |\varepsilon_2| = 1.3$, $\Delta\varphi = 4°$) has been used to predict the Eulerian drift throughout the boundary layer. In particular, the following data sets have been considered: *Van Doorn and Godefroy*'s [1978] test RA/RB (VD), *Mathisen and Madsen*'s [1996b] tests a,b,c (MMa, b, c), and *Villaret and Perrier*'s [1992] tests 35 and 39 (VP35, 39). *Marin and Sleath*'s [1994] data sets have been excluded from this comparison for the reason given in section 5.1.

Comparisons between the predictions of the standard model (solid lines) and the drift data (symbols) are shown in Figures 9, 10, and 11. In some cases, a small change in the model coefficients was found to improve the overall fit to the data; these "adjusted" model results are also shown (dash-dotted lines). The classical LH solution is shown for comparison in each figure. In addition, in the cases of VD and VP39, the profile given by *Trowbridge and Madsen*'s [1984b] model (TM) is also included. Although it should be emphasized that this model is being used here outside its range of validity ($A_0/k_s \gtrsim 30$), the two cases chosen are those for which A_0/k_s was relatively large (>4).

In Figure 9, the comparison between the standard model and the VD data is generally satisfactory. However, the maximum near-bed drift is overestimated by the model, while the height at which the direction of drift reverses is underestimated. Significantly better agreement can be achieved by reducing the values of the eddy viscosity coefficients to $|\varepsilon_1| = 1.0$ and $|\varepsilon_2| = 0.33$, while maintaining the phase lead as $\Delta\varphi = 4°$. This improvement suggests a possible dependence of the model coefficients upon the relative roughness (since $A_0/k_s = 4.1$ in VD), as well as upon the degree of wave asymmetry ($B = 0.22$ in VD). This is discussed further in section 6. The agreement between the TM model (run here with $B = 0.22$) and the data is quite good in this case and certainly much better than obtained by use of the LH model.

The comparisons between the standard model and *Mathisen and Madsen*'s [1996b] data are shown in Figure 10. For test MMa (Figure 10a), the boundary layer thickness is clearly underestimated in comparison with the data. In this case, it was found necessary to enhance δ_w by a factor of 1.8. This suggests that in the lower range of relative roughness (here $A_0/k_s \sim 0.3$), the method used to estimate δ_w (section 5.2.2) may no longer be valid (see section 6). After enhancement of

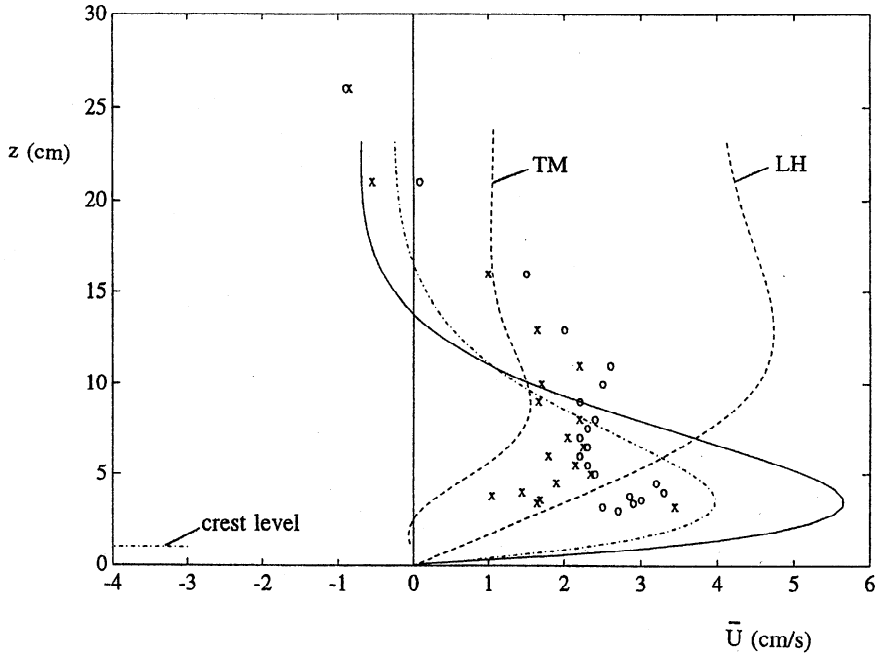

Figure 9. Comparison between measured and predicted vertical profiles of the Eulerian drift for the data (test RA/RB) of *Van Doorn and Godefroy* [1978]. The symbols indicate measurements made above the crests (crosses) and troughs (circles) of the roughness elements. The origin of z is located at the level midway between the crests and troughs, and the height of the crests of the roughness elements is indicated by the dash-dotted line at the bottom left. The predicted profiles are from the standard model (solid line), the adjusted model (dash-dotted line), and LH model (dashed line).

the boundary layer thickness, the agreement between the measured drift profile and the standard model is quite good, both the outer flow drift and also the level at which the flow reverses being reproduced accurately. For test MMb (Figure 10b), the agreement between the standard model and the measurements is generally satisfactory, though there is substantial scatter in the data in this case. For test MMc (Figure 10c), the agreement between the standard model and the Eulerian drift measurements is improved by reducing the value of $|\varepsilon_2|$ from 1.3 to 0.43, while keeping the other coeffi-

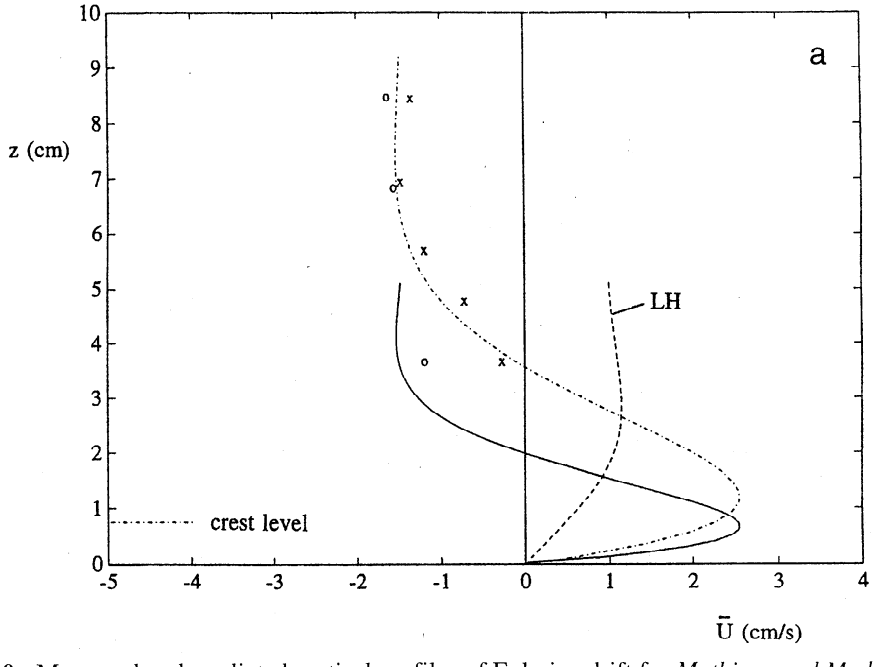

Figure 10. Measured and predicted vertical profiles of Eulerian drift for *Mathisen and Madsen*'s [1996b] tests (a) MMa, (b) MMb, and (c) MMc. The definitions of the symbols and lines are the same as in Figure 9.

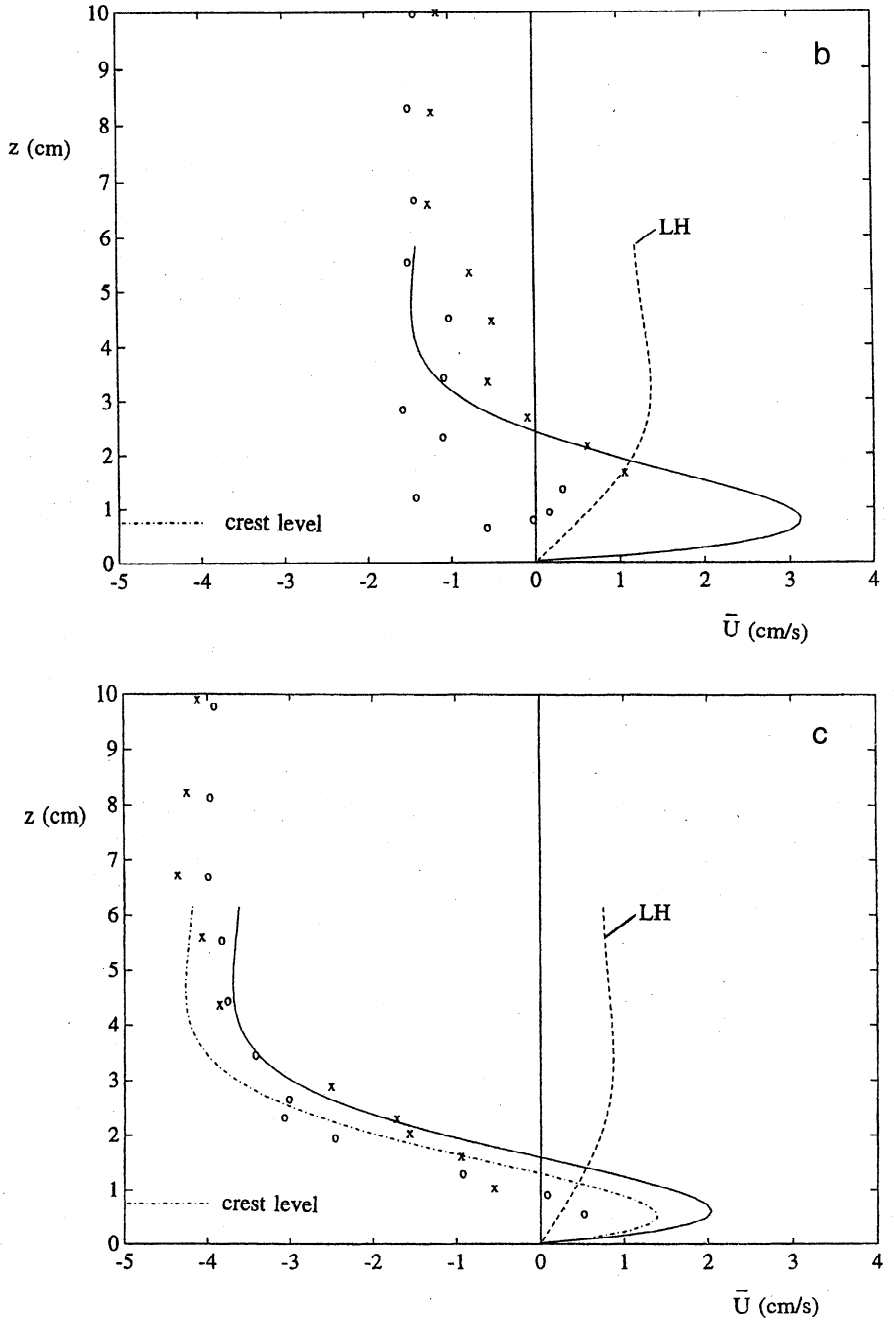

Figure 10. (continued)

cients unchanged. This reduction in $|\varepsilon_2|$ can be justified in terms of the large degree of wave asymmetry in this case ($B > 0.15$) (see section 6).

The comparisons between the standard model and the VP35 and VP39 data (Figures 11a and 11b, respectively) are generally satisfactory. Both the outer flow drift and the height of reversal are well reproduced, such that no adjustment of the model coefficients is beneficial in these cases. The agreement between the TM model and the data is not as good in the case of VP39.

6. Discussion

In the standard time-varying eddy viscosity model, the magnitude of the coefficients $|\varepsilon_1|$ and $|\varepsilon_2|$ has been assumed to remain constant. On the basis of our analysis of the outer flow Eulerian drift, we found that $|\varepsilon_1| = 1.3 \pm 0.2$ with $\Delta\varphi = 4°$, while for $|\varepsilon_2|$ we used the earlier estimate of DV97, namely, $|\varepsilon_2| = 1.3$. The resulting standard model has been shown to make reasonable estimates for both the outer flow Eulerian drift and also the vertical drift profile. However, for some of the data sets, a slight adjustment to the model coefficients was found to improve the overall fit to the profiles. Since a dependence of the coefficients upon the degree of asymmetry B, as well as on the relative roughness A_0/k_s, may be expected physically, we now consider these possibilities in turn.

6.1. Dependence of the Drift on A_0/k_s

First, in the very rough turbulent range ($A_0/k_s \sim 0.3$, test MMa), it was found necessary to increase the boundary layer

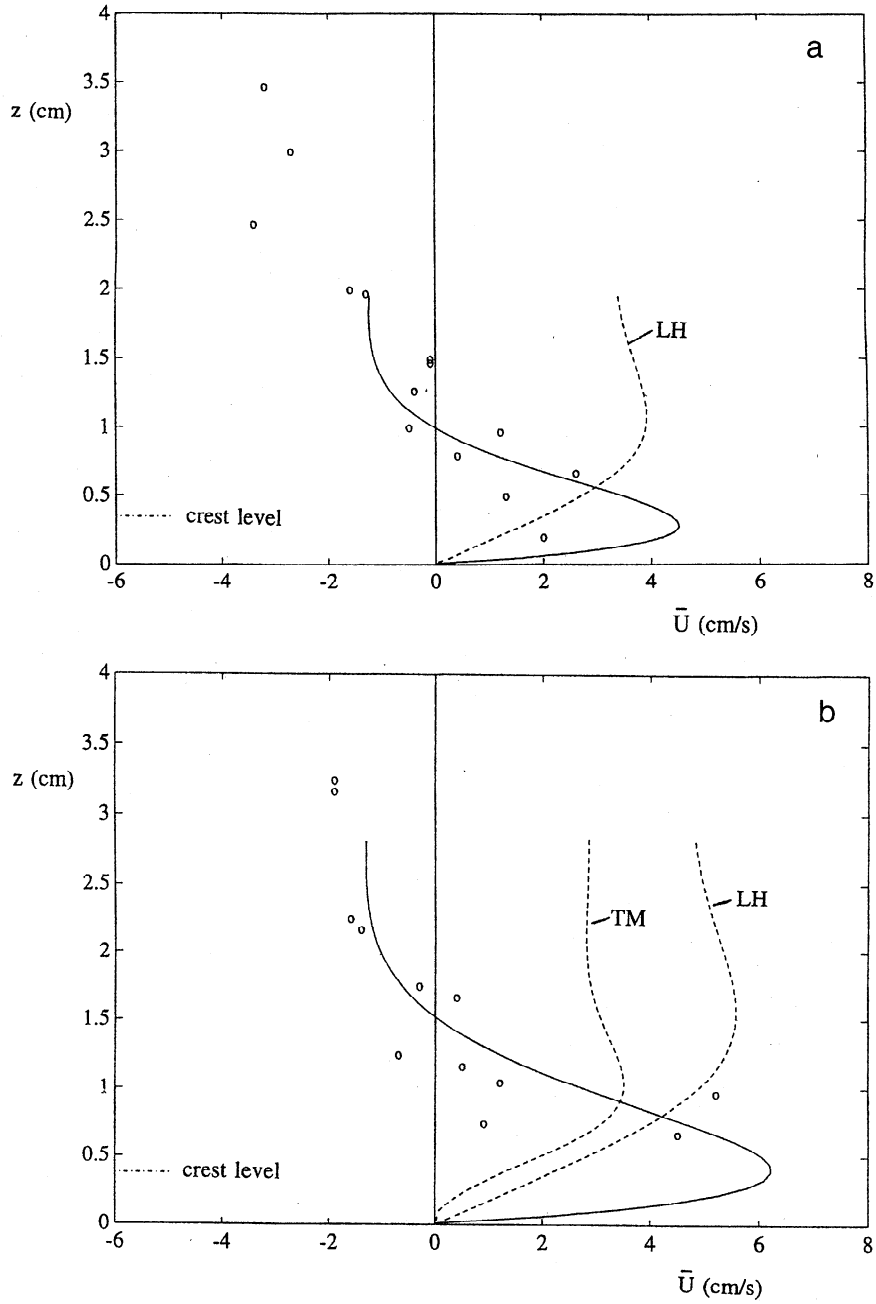

Figure 11. Measured and predicted vertical profiles of Eulerian drift for *Villaret and Perrier*'s [1992] tests (a) VP35 and (b) VP39. The definitions of the symbols and lines are the same as in Figure 9. No adjusted model runs were found beneficial in this case.

thickness by a factor of 1.8. The underestimate of δ_w by the standard model may be due to the fact that *Nielsen*'s [1992] formula (equation (56)) is not valid in these conditions. (This formula is based only on data for which $A_0/k_s > 2$.) Another possibility is that the boundary layer thickess should have been scaled on the maximum value of eddy viscosity during the wave cycle, rather than on the cycle-mean value (equation (55)).

Second, in the intermediate range ($A_0/k_s > 2.5$, test VD), it was found necessary to reduce the magnitude of both of the time-varying components of K. In fact, this is not surprising, given that the eddy-shedding process should become less important as the bed roughness decreases. In the limit of a flat rough bed ($A_0/k_s > 30$), *Trowbridge and Madsen* [1984a] assumed that $|\varepsilon_2| = 0.4$.

6.2. Dependence of the Drift on B

The relative magnitude of the two peaks in the standard time-varying eddy viscosity model was assumed to remain constant (Figure 7). In fact, this is a very crude approximation, since the degree of wave asymmetry B is expected to have some influence on K. It has been noted previously that for very asymmetrical waves ($B > 0.2$), secondary vortex ejection following the passage of the wave trough may no longer occur [*Perrier*, 1996]. This effect can be reproduced in the present simple model by decreasing the relative magnitude of the ε_2

component. For example, in both tests MMc and VD, which correspond to the largest values of B (0.18 and 0.21, respectively), better agreement is achieved by reducing the quotient $|\varepsilon_2|/|\varepsilon_1|$ to about ⅓. The time-varying eddy viscosity model then contains only one peak per wave cycle.

Owing to the lack of suitable data, some uncertainty remains about the range of validity of the present model and about the precise behavior of the model coefficients as the value of B is varied. Nevertheless, there is sufficient evidence to suggest the following general trends for the model coefficients in the very rough turbulent regime ($A_0/k_s \lesssim 2$). For symmetrical waves ($B = 0$), we expect that $|\varepsilon_1| = 0$ and $|\varepsilon_2| \approx 1.3$ (with $\varphi_2 = \pi$). In the range $0 < B \lesssim 0.05$, $|\varepsilon_1|$ increases steadily to a maximum value of about 1.3 at $B \approx 0.05$. For weakly asymmetrical waves in the range $0.05 \lesssim B \lesssim 0.1$, $|\varepsilon_1|$ and $|\varepsilon_2|$ both then remain constant (and equal to about 1.3) with phase angles given by (54). As the waves become still more asymmetrical in the range $0.1 \lesssim B \lesssim 0.15$, the coefficient $|\varepsilon_2|$ decreases such that for $B \gtrsim 0.15$, $|\varepsilon_1| = 1.3$ and $|\varepsilon_2| \approx ⅓|\varepsilon_1|$.

In the very rough turbulent regime ($A_0/k_s \lesssim 2$), momentum transfer is dominated by the eddy-shedding process, and this may be represented by the above convective eddy viscosity. As A_0/k_s increases in the range (2, 30), the role of coherent vortex structures progressively decreases (whatever the value of B is), while the importance of random turbulent fluctuations increases. Finally, for $A_0/k_s \gtrsim 30$, momentum transfer is dominated by turbulent processes and a modeling approach such as that of *Trowbridge and Madsen* [1984b] becomes appropriate. For symmetrical waves, Trowbridge and Madsen found that the near-bed Eulerian drift increases slightly in magnitude as A_0/k_s decreases, tending to $\overline{U}_\infty c/U_0^2 \approx 0.75$ as $A_0/k_s \to 30$. In obtaining this result in the symmetrical wave limit, Trowbridge and Madsen included no time variation in K. According to our solution, this trend of increasing nondimensional drift does not continue as A_0/k_s decreases in the range $A_0/k_s < 30$.

In relation to the vertical structure of K in turbulent flows, it was suggested by *Trowbridge and Madsen* [1984a] that the time-varying component of K may decay more rapidly with distance above the bed than the steady component. Here, for rippled and very rough beds, we have assumed the same (i.e., constant) vertical structure for both the steady and unsteady components of K, there being no clear empirical evidence to suggest an alternative structure. However, it is possible that the time-varying component of K does, in fact, vary with height, particularly in the outer part of the oscillatory boundary layer (i.e., above the near-bed vortex-dominated layer).

Finally, as noted in section 4.2 the simple convective eddy viscosity defined by (7), which was assumed (equation (15)) to include only harmonics up to the second in K, becomes negative for short intervals during the wave cycle (Figure 7). This is a consequence of our analysis of the data of *Ranasoma* [1992]. If, in general, the eddy viscosity is considered to be proportional to a (positive) velocity scale and also a (positive) length scale characterizing the turbulent motion, then, as pointed out by *Rodi* [1984], even in relatively simple flows, the eddy viscosity concept breaks down. For example, in simple wall jets, regions exist where the shear stress and velocity gradient have opposite signs, implying a negative eddy viscosity which, according to *Rodi* [1984, p.11] is "mathematically possible, but not physically meaningful". However, the above notion of an eddy viscosity, which involves a strict analogy with molecular diffusion, need not be adopted. In fact, the idea of a negative eddy viscosity has been invoked many times as a possible explanation for common instabilities in geophysical flows [see *Frisch* [1995, chapter 9, and references therein]]. For example, *Kraichnan* [1976] obtained negative values for the eddy viscosity, which he used to interpret the reverse flow of energy to larger scales in the "inverse cascade" of two-dimensional turbulence. In the context of measurements made in oscillatory flow above rippled beds, *Sato et al.* [1987] obtained negative values of eddy viscosity in regions where the flow was accelerating, and *Marin and Belorgey* [1994] reported regions of "negative turbulent energy production" close to the bottom. In fact, at certain instants during the wave cycle, the results of this latter study suggest negative production in the spatial-mean sense, a phenomenon possibly connected with a negative viscosity. However, for the reason given in section 4.2, we do not seek here to attach such a definite interpretation to the short intervals of negative viscosity implied by our present definition of K.

7. Conclusions

A simple, analytical model has been presented for the prediction of the near-bed Eulerian drift induced by weakly asymmetrical waves ($B \lesssim 0.2$) above very rough and rippled beds ($A_0/k_s \lesssim 5$). Above such beds, momentum transfer is dominated by the spatially well organized process of vortex shedding, rather than by random turbulent processes. A simplified, time-varying convective eddy viscosity K has been defined here (equation (7)) to characterize this vortex-shedding process in a standard, one-dimensional, gradient diffusion framework. This approach was motivated by the observation that the measured spatial-mean velocity field above a rippled bed preserves features of the classical Stokes' shear wave solution. The present convective eddy viscosity includes symmetrical and asymmetrical time-varying components, with phase angles such that the peak value of K occurs at about the time of flow reversal following the passage of each (steep) wave crest.

The Eulerian drift in the bottom wave boundary layer (equation (50)) comprises three contributions that arise from the relationship between the time-varying velocity and eddy viscosity fields. The first contribution (equation (43)) arises from the wave Reynolds stress associated with the lowest-order velocity field, while the second and third contributions (equations (47) and (49)) are asymmetry terms arising from the time-varying components of K. For typical weakly asymmetrical waves, the Eulerian drift profile comprises (1) a near-bed jet in the direction of wave advance; (2) a level of zero drift within the boundary layer; and (3) a reversal in the direction of drift, which then extends to the edge of the boundary layer.

The model predictions have been compared with results from five flume investigations involving asymmetrical waves above very rough and rippled beds. The reversal in the drift noted above was evident at the edge of the boundary layer in almost all of these experiments, its magnitude depending upon the degree of wave asymmetry B and also on the relative bed roughness A_0/k_s. The model presented here shows good agreement with the measured vertical drift profiles for ranges of values of B and A_0/k_s of practical importance. The results obtained have significant implications both for the magnitude and direction of net sediment transport in the coastal zone and also for vertical profiles of residual currents in the water column as a whole.

Appendix: First-Order Solution When ε_2 is Not "Small"

The governing equation (17) for the first harmonic of the velocity field was obtained earlier as a perturbation solution in

which ε_2 was assumed to be small. Since, in practice, ε_2 may not be small, it may be noted that (17) can be solved directly as follows. If a solution is sought for the defect velocity $U_0F(z)\exp(i\theta)$, where function $F(z)$ is defined by

$$U_1 = U_0\,[1 - F(z)]\,, \tag{A1}$$

and if F is written in the form

$$F = G_1 + iG_2\,, \qquad (G_{1,2}\ real) \tag{A2}$$

then two coupled equations are obtained for G_1 and G_2 after (A2) is substituted into (17), the real and imaginary parts of the equation yielding, respectively,

$$\begin{aligned} -\alpha_0^2 G_2 &= -\tfrac{1}{4}\varepsilon_R \frac{d^2G_1}{dz^2} + \tfrac{1}{4}\varepsilon_I \frac{d^2G_2}{dz^2} - \tfrac{1}{2}\frac{d^2G_1}{dz^2} \\ -\alpha_0^2 G_1 &= -\tfrac{1}{4}\varepsilon_R \frac{d^2G_2}{dz^2} - \tfrac{1}{4}\varepsilon_I \frac{d^2G_1}{dz^2} - \tfrac{1}{2}\frac{d^2G_2}{dz^2} \end{aligned} \tag{A3}$$

where $\varepsilon_R = |\varepsilon_2|\cos\varphi_2$ and $\varepsilon_I = |\varepsilon_2|\sin\varphi_2$ are the real and imaginary parts of $\varepsilon_2 = |\varepsilon_2|\exp(i\varphi_2)$, respectively, and $\alpha = (\omega/K_0)^{1/2}$. Eliminating G_2 leads to the following fourth-order equation for G_1:

$$\left(1 - \tfrac{1}{4}|\varepsilon_2|^2\right)\frac{d^4G_1}{dz^4} + 4\alpha^2 G_1 = 0\,. \tag{A4}$$

The solution for G_1 has the form

$$G_1 = Ae^{-\beta z}\cos\beta z + Be^{-\beta z}\sin\beta z\,, \tag{A5}$$

where A and B are constants and in which β is given by

$$\beta_0^4 = \frac{\alpha_0^4}{\left(1 - \tfrac{1}{4}|\varepsilon_2|^2\right)}\,. \tag{A6}$$

It is apparent from (A6) that the shear wavenumber β is smaller than the wavenumber α in the perturbation solution, implying that the boundary layer becomes thinner as ε_2 is increased. After some further algebra, the solution may be written as

$$U_1 = U_0\left\{1 - e^{-\beta z}\cos\beta z + \frac{[-\varepsilon_I + i(2 + \varepsilon_R)]}{\sqrt{4 - |\varepsilon_2|^2}}\,e^{-\beta z}\sin\beta z\right\}. \tag{A7}$$

As $\varepsilon_2 \to 0$, it is apparent that $\beta \to \alpha$ and that (A7) reverts to (21).

If (A7) is used in (37) instead of (21) in order to determine the contribution to the Eulerian drift arising from wave Reynolds stresses, the drift profile may be expressed in the form (see (42)):

$$\overline{U^{(1)}}|_m = \overline{U_s}|_m\left[\frac{2 + \varepsilon_R}{\sqrt{4 - |\varepsilon_2|^2}}\right], \tag{A8}$$

where $\overline{U}_s|_m$ is equal to the drift profile given by (39), subject to the replacement of α by β throughout this equation.

Acknowledgments. This study was initiated as part of the MAST2 G8-M Coastal Morphodynamics project, supported financially by the Commission of the European Communities, Directorate General for Science, Research and Development under contract MAS2-CT92-0027. The first author would like to thank the Laboratoire National d'Hydraulique, E.D.F., for its hospitality during the course of this study.

References

Bijker, E. W., J. P. T. Kalkwijk, and T. Pieters, Mass transport in gravity waves on a sloping bottom, in *Proceedings of the 14th International Conference on Coastal Engineering,* pp. 447-465, Am. Soc. of Civ. Eng., New York, 1974.

Block, M. E., A. G. Davies, and C. Villaret, Suspension of sand in oscillatory flow above ripples: Discrete vortex model and laboratory experiments, in *Sediment Transport Mechanisms in Coastal Environments and Rivers, EUROMECH 310*, edited by M. Belorgey, R. D. Rajaona, and J. F. A. Sleath, pp. 37-52, World Sci., River Edge, N. J., 1994.

Brebner, A., J. A Askew, and S. W. Law, The effect of roughness on the mass-transport of progressive gravity waves, in *Proceedings of the 10th International Conference on Coastal Engineering*, pp. 175-184, Am. Soc. of Civ. Eng., New York, 1966.

Davies, A. G., and Z. Li, Modelling sediment transport beneath regular symmetrical and asymmetrical waves above a plane bed, *Cont. Shelf Res.*, *17*(5), 555-582, 1997.

Davies, A. G., and C. Villaret, Oscillatory flow over rippled beds: Boundary layer structure and wave-induced Eulerian drift, in *Gravity Waves in Water of Finite Depth, Adv. Fluid Mech.*, edited by J. N. Hunt, chap. 6, pp. 215-254, Comput. Mech., Billerica, Mass., 1997.

Davies, A. G., and C. Villaret, Wave-induced currents above rippled beds and their effects on sediment transport, in *Physics of Estuaries and Coastal Seas*, edited by J. Dronkers and M. Scheffers, pp. 187-199, A.A. Balkema, Brookfield, Vt., 1998.

Frisch, U., *Turbulence*, Cambridge Univ. Press, New York, 1995.

Johns, B., On the mass transport induced by oscillatory flow in a turbulent boundary layer, *J. Fluid Mech., 43*(1), 177-185, 1970.

Kraichnan, R. H., Eddy viscosity in two and three dimensions, *J. Atmos. Sci., 33*, 1521-1536, 1976.

Longuet-Higgins, M. S., Mass transport in water waves, *Philos. Trans. R. Soc. London, Ser. A, 245*(903), 535-581, 1953.

Longuet-Higgins, M. S., The mechanics of the boundary-layer near the bottom in a progressive wave, in *Proceedings of the 6th International Conference on Coastal Engineering*, pp. 184-193, Am. Soc. of Civ. Eng., New York, 1958.

Marin, F., and M. Belorgey, Flow regime and eddy structures into a boundary layer generated by the swell above a rippled bed, in *Sediment Transport Mechanisms in Coastal Environments and Rivers, EUROMECH 310*, edited by M. Belorgey, R. D. Rajaona, and J. F. A. Sleath, pp. 231-245, World Sci., River Edge, N. J., 1994.

Marin, F., and J. F. A. Sleath, Mass transport over rippled beds, in *Sediment Transport Mechanisms in Coastal Environments and Rivers, EUROMECH 310*, edited by M. Belorgey, R. D. Rajaona, and J. F. A. Sleath, pp. 246-254, World Sci., River Edge, N. J., 1994.

Mathisen, P. P., and O. S. Madsen, Waves and currents over a fixed rippled bed, 1, Bottom roughness experienced by waves in the presence and absence of currents, *J. Geophys. Res., 101*(C7), 16,533-16,542, 1996a.

Mathisen, P. P., and O. S. Madsen, Waves and currents over a fixed rippled bed, 2, Bottom and apparent roughness experienced by currents in the presence of waves, *J. Geophys. Res., 101*(C7), 16,543-16,550, 1996b.

Nielsen, P., *Coastal Bottom Boundary Layers and Sediment Transport,* 324 pp., World Sci., River Edge, N. J., 1992.

Nielsen, P., and Z.-J. You, Eulerian mean velocities under non-breaking waves on horizontal bottoms, in *Proceedings of the 25th International Conference on Coastal Engineering*, pp. 4066-4078, Am. Soc. of Civ. Eng., New York, 1996.

Perrier, G., Numerical modelling of the transport of non-cohesive sediments by waves and currents over a rippled bed, *Rep. HE-42/96/005*, 380 pp., Electr. de France, Chatou, 1996.

Perrier, G., E. A. Hansen, C. Villaret, R. Deigaard, and J. Fredsoe,

Flow and sediment transport over a rippled bed in waves and current, in *Proceedings of the 24th International Conference on Coastal Engineering*, pp. 2043-2057, Am. Soc. of Civ. Eng., New York, 1994.

Ranasoma, K. I. M., Measurements in combined oscillatory and steady flow over rippled beds, Ph.D. thesis, Univ. of Cambridge, Cambridge, England, 1992.

Ranasoma, K. I. M., and J. F. A. Sleath, Velocity measurements close to rippled beds, in *Proceedings of the 23rd International Conference on Coastal Engineering*, pp. 2383-2396, Am. Soc. of Civ. Eng., New York, 1992.

Ribberink, J. S., and A. A. Al-Salem, Sheet flow and suspension of sand in oscillatory boundary layers, *Coastal Eng., 25*, 205-225, 1995.

Rodi, W., *Turbulence Models and Their Application in Hydraulics - A State of the Art Review*, A. A. Balkema, Brookfield, Vt., 1984.

Sato, S., K. Shimosako, and A. Watanabe, Measurements of oscillatory turbulent boundary layer flow above ripples with a laser-Doppler velocimeter, *Coastal Eng. Jpn., 30*, 1, 1987.

Sleath, J. F. A., Measurements of mass transport over a rough bed, in *Proceedings of the 19th International Conference on Coastal Engineering*, pp.1149-1160, Am. Soc. of Civ. Eng., New York, 1984.

Sleath, J. F. A., Turbulent oscillatory flow over rough beds, *J. Fluid Mech., 182,* 369-409, 1987.

Sleath, J. F. A., Velocities and shear stresses in wave-current flows, *J. Geophys. Res., 96*(C8), 15,237-15,244, 1991.

Swart, D. H., Predictive equations regarding coastal transports, in *Proceedings of the 15th International Conference on Coastal Engineering*, pp. 1113-1132, Am. Soc. of Civ. Eng., New York, 1976.

Trowbridge, J. H., and O. S. Madsen, Turbulent wave boundary layers, 1, Model formulation and first-order solution, *J. Geophys. Res., 89*(C5), 7989-7997, 1984a.

Trowbridge, J. H., and O. S. Madsen, Turbulent wave boundary layers, 2, Second-order theory and mass transport, *J. Geophys. Res., 89*(C5), 7999-8007, 1984b.

Van Doorn, T., and H. W. H. E. Godefroy, Experimental investigation of the bottom boundary layer under periodic progressive water waves, *Rep. M1362, part I*, Delft Hydraul., Delft, Netherlands, 1978.

Villaret, C., and B. Latteux, Entrainment and transport of fine sand by combined waves and current: An experimental study, in *Proceedings of the 23rd International Conference on Coastal Engineering*, pp. 2500-2512, Am. Soc. of Civ. Eng., New York, 1992.

Villaret, C., and G. Perrier, Transport of fine sand by combined waves and current: An experimental study, *Rep. HE-42/92.68,* 81 pp., Electr. de France, Chatou, 1992.

A. G. Davies, School of Ocean Sciences, University of Wales (Bangor), Menai Bridge, Anglesey LL59 5EY, Wales, United Kingdom. (e-mail: a.g.davies@sos.bangor.ac.uk)

C. Villaret, Laboratoire National d'Hydraulique, E.D.F., 6 Quai Watier, B.P. 49, 78400 Chatou, France. (e-mail: Catherine.Villaret@edf.fr)

(Received July 25, 1997; revised June 23, 1998; accepted July 28, 1998.)